

JGR Earth Surface

RESEARCH ARTICLE

10.1029/2022JF006599

Key Points:

- Lake-terminating glaciers flow 1.7 times and tidewater glaciers 2.3 times faster than the land-terminating glaciers
- Monthly ice speed variations are largely synchronous across the Peninsula irrespective of terminus type
- A glacier outburst flood at Bear Glacier caused both a short-term and a longer-term speed-up of the glacier's lower part

Supporting Information:

Supporting Information may be found in the online version of this article.

Correspondence to:

R. Yang and W. Guo,
ryt@lzb.ac.cn;
ruitang.yang@geo.uio.no;
guowq@lzb.ac.cn

Citation:

Yang, R., Hock, R., Kang, S., Guo, W., Shangguan, D., Jiang, Z., & Zhang, Q. (2022). Glacier surface speed variations on the Kenai Peninsula, Alaska, 2014–2019. *Journal of Geophysical Research: Earth Surface*, 127, e2022JF006599.
<https://doi.org/10.1029/2022JF006599>

Received 12 JAN 2022

Accepted 7 MAR 2022

Author Contributions:

Conceptualization: Ruitang Yang, Regine Hock, Shichang Kang, Wanqin Guo
Data curation: Ruitang Yang
Formal analysis: Ruitang Yang
Funding acquisition: Ruitang Yang, Shichang Kang
Investigation: Ruitang Yang, Regine Hock
Methodology: Ruitang Yang, Regine Hock
Project Administration: Shichang Kang
Resources: Ruitang Yang, Donghui Shangguan, Qibing Zhang
Software: Ruitang Yang, Zongli Jiang
Supervision: Regine Hock, Shichang Kang, Wanqin Guo
Validation: Ruitang Yang

© 2022. American Geophysical Union.
All Rights Reserved.

Glacier Surface Speed Variations on the Kenai Peninsula, Alaska, 2014–2019

Ruitang Yang^{1,2,3,4} , Regine Hock^{2,3} , Shichang Kang^{1,4} , Wanqin Guo¹,
Donghui Shangguan¹ , Zongli Jiang⁵ , and Qibing Zhang⁶

¹State Key Laboratory of Cryospheric Science, Northwest Institute of Eco-Environment and Resources, Chinese Academy of Sciences, Lanzhou, China, ²Department of Geosciences, University of Oslo, Oslo, Norway, ³Geophysical Institute, University of Alaska Fairbanks, Fairbanks, AK, USA, ⁴University of Chinese Academy of Sciences, Beijing, China, ⁵School of Resource Environment and Safety Engineering, Hunan University of Science and Technology, Xiangtan, China, ⁶College of Geography and Tourism, Hunan University of Arts and Science, Changde, China

Abstract To characterize the spatiotemporal variations of glacier surface speed on the Kenai Peninsula, Alaska ($\sim 3,900 \text{ km}^2$), we derived 92 surface speed fields between October 2014 and December 2019 using intensity offset tracking on Sentinel-1 data. On average, speeds are 50% greater in spring (March–May) than the annual mean (69 m a^{-1}) while winter speeds are close to the annual mean. While marine-terminating glaciers have their maximum speed near the terminus, both land- and lake-terminating glaciers flow fastest around the median glacier elevation. On average, the lake-terminating and tidewater glaciers flow 1.7 and 2.3 times faster than the land-terminating glaciers, respectively. Monthly variations over the 5-year period are strikingly synchronous regardless of terminus type suggesting that regional-scale meteorological drivers govern the temporal variability. Mean annual speeds fluctuate roughly $\pm 10\%$ of the period mean without an apparent trend. At lake-terminating Bear Glacier, a short-term tripling in ice speed in fall 2019 over the area below an ice-dammed lake coincides with an observed glacier lake outburst flood (GLOF). An earlier GLOF caused a persistent breach of the beach barrier between the proglacial lake and ocean which likely led to overall speed-up of the lower glacier part throughout 2019. A significant speedup was also observed at the lower part of the lake-terminating Ellsworth Glacier and attributed to rapid glacier retreat and lake expansion, probably further amplified by the terminus area becoming buoyant and a large tabular iceberg breaking off. Our results highlight the impact of GLOFs and proglacial characteristics in spatial and temporal glacier speed variations.

Plain Language Summary

Glaciers constantly move but the speed varies with time and space. We use satellite data to calculate the surface ice speed variations of all glaciers on the Kenai Peninsula, Alaska ($\sim 3,900 \text{ km}^2$), between October 2014 and December 2019. On average, the glacier speed is 50% higher in spring than the annual average. Overall, the lake-terminating glaciers flow 70% faster, and marine-terminating glaciers more than 100% faster than the land-terminating glaciers. Over the 5-year period, all glaciers regardless of terminus type tended to speed up or slow down simultaneously, probably driven by large-scale variations in weather governing the water supply to the drainage system. The lower part of Bear Glacier tripled in speed in fall 2019 when an ice-dammed lake suddenly drained through the glacier. Another glacier outburst flood in 2018 led to a breach of the beach barrier between the large lake at the glacier terminus and the ocean which might have caused the considerable speedup of the lower glacier part throughout 2019.

1. Introduction

Ice flow plays a fundamental role in glacier dynamics and mass balance as well as glacier hazards. Ice velocity highly varies on many time scales, such as decadal and annual time scales, or over just a few days or even a few hours (Iken, 1981; Van den Broeke et al., 2009; Willis, 1995). Velocities can range from a few centimeters per year to several kilometers per year (Rignot & Mouginot, 2012). Thus, there is a need for regional-scale assessments of glacier velocities with high spatiotemporal resolution. Since in situ observations are logistically challenging and limited to individual glaciers, remote sensing methods have increasingly been used to map glacier velocities on larger scales. Interferometric Synthetic Aperture Radar (InSAR), and Differential Interferometric SAR (DInSAR) have been widely used on SAR data (Gourmelen et al., 2011; Kumar et al., 2011; Rignot et al., 1996; Sánchez-Gámez & Navarro, 2017), while offset tracking has been shown to be effective for both optical (Fahnestock et al., 2016; Kääb, 2005; Wu et al., 2020) and SAR data (Muto & Furuya, 2013; Schellenberger et al., 2015).

Visualization: Ruitang Yang
Writing – original draft: Ruitang Yang,
Regine Hock
Writing – review & editing: Ruitang
Yang, Regine Hock, Shichang Kang,
Wanqin Guo

In recent decades, many studies have investigated spatiotemporal variations of ice velocity of the entire ice sheet or outlet glaciers of the Greenland (Ahlström et al., 2013; Rosenau et al., 2015; Vijay et al., 2019) and Antarctic ice sheets (Jawak et al., 2019; Mouginot et al., 2017; Zhou et al., 2017). Most studies outside the ice sheets have focused on individual glaciers or smaller glacier regions (Mair et al., 2001; Neelmeijer et al., 2014; Purdie et al., 2008; Satyabala, 2016; Tsutaki et al., 2019). Only few studies have examined ice velocities of mountain glaciers on larger scales in detail (e.g., West Kunlun Mts. (Yasuda & Furuya, 2013), Karakoram region (Rankl et al., 2014), High Mountain Asia (Dehecq et al., 2019), Patagonian Icefields (Mouginot & Rignot, 2015), Canadian High Arctic (Van Wychen et al., 2020), Circum-Arctic (Strozzi et al., 2017), high mountain regions in the European Alps, Peru and New Zealand (Millan et al., 2019), and global (Millan et al., 2022)). In Alaska, Burgess et al. (2013) presented the first comprehensive flow map for glaciers in Central Alaska (including the Kenai Peninsula), but speeds were based on winter images only. Melkonian et al. (2014) derived surface velocities by SAR offset tracking, for the Juneau Icefield, while Armstrong et al. (2017) employed optical offset tracking to derive velocity fields for South Central Alaska glaciers, and Altena et al. (2019) extracted glacier velocity over southern Alaska and Yukon from Landsat data. Other studies have determined ice velocity fields of larger ice caps for the purpose of computing frontal ablation rates rather than a detailed analysis of ice motion (e.g., Antarctic periphery (Osmanoglu et al. (2013); Osmanoglu et al. (2014)) and Canada's Queen Elizabeth Islands (Van Wychen et al., 2014)).

Recently, the Global Land Ice Velocity Extraction from Landsat 8 (GoLIVE) (Scambos et al., 2016) and the NASA MEASUREs ITS_LIVE project (Gardner et al., 2020) have released global velocity data sets based on Landsat images by offset tracking. However, the spatial or temporal coverage of these data on the Kenai Peninsula is insufficient to analyze the spatiotemporal variations in detail.

In this study, we use offset tracking on a sequence of Sentinel-1 A/B SAR data to derive glacier surface speed fields with high temporal resolution and investigate the spatial and temporal (seasonal and interannual) ice flow variations of all glaciers ($\sim 3,900 \text{ km}^2$) on the Kenai Peninsula, Alaska, for the period October 2014 to December 2019. We focus on differences between tidewater, lake-, and land-terminating glaciers and also analyze the effects of Glacier Lake Outburst Floods (GLOF) and other environmental factors on ice flow.

2. Study Area and Data

2.1. Study Area

The Kenai Peninsula is situated in south-central Alaska between the Cook Inlet and the Gulf of Alaska (Figure 1). A wet maritime climate dominates in the east and south of the Peninsula and a continental climate in the north and west (Le Bris et al., 2011). Glaciers in this region cover an area of $\sim 3,900 \text{ km}^2$ ($\sim 5\%$ of the total Alaskan glacier area) and range in elevation from 0 to $\sim 2,000 \text{ m a.s.l}$. The mean ice thickness is $\sim 240 \text{ m}$, and the maximum exceeds 1,400 m on the Harding Icefield (Millan et al., 2022). There are $\sim 1,460$ individual glaciers in this region, including 11 tidewater glaciers (23% of total glacier area) and 18 lake-terminating glaciers (34%; updated from the Randolph Glacier Inventory v6.0; RGI Consortium, 2017; Table S1 in Supporting Information S2). According to Wiles and Calkin (1992), glaciers on the Kenai Peninsula have experienced widespread recession since the Little Ice Age, while in recent decades they experienced on average a $12\% \pm 3\%$ area shrinkage (1986–2016) and specific mass changes of $-0.94 \pm 0.12 \text{ m w.e. a}^{-1}$ (2005–2014) (Yang et al., 2020).

2.2. Data

2.2.1. Sentinel-1 A/B

Sentinel-1A was launched in April 2014 and the twin satellite Sentinel-1B in April 2016 by the European Space Agency (ESA), providing continuous all-weather, dusk-and-dawn images at C-band (5.4 GHz). The initial orbit repeat cycle of 12 days was halved with the launch of Sentinel-1b. The orbit is sun synchronous and near polar.

We used 92 pairs of Sentinel-1A and 1B single-look complex (SLC) SAR TOPS images between October 2014 and December 2019 (retrieved from ASF DAAC access date: 5 May 2020, processed by ESA, <https://search.asf.alaska.edu/>) to track the seasonal and annual glacier speed changes on the Kenai Peninsula. The images have a $5 \times 20 \text{ m}$ resolution and were acquired in the interferometric wide (IW) mode with VV/VV + VH polarization (Table S3 in Supporting Information S2, Figure 1).

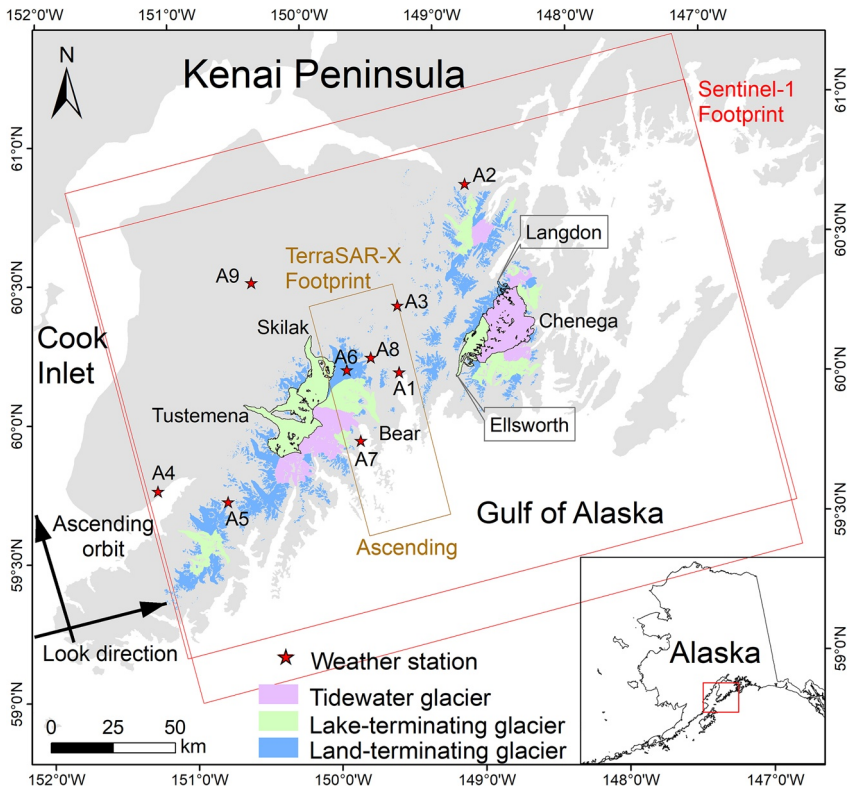


Figure 1. Map of all glaciers on the Kenai Peninsula. Also shown are the footprints for Sentinel-1A/B, and TerraSAR-X SAR data over the study region and the location of available weather stations (Table S2 in Supporting Information S2).

2.2.2. TerraSAR-X

TerraSAR-X images were used to validate results over a subregion covered by both sensors. The TerraSAR-X satellite was launched in June 2007 and provided X-band SAR data with 11 days repeat pass orbits. Two TerraSAR-X images, gained in Stripmap mode with 3×3 m resolution with HH polarization and ascending orbit (Table S3 in Supporting Information S2), were used to derive surface speed through the offset tracking method for the period 23 September to 4 October 2016. We used the data to evaluate our Sentinel-1 speed data set over the closest overlapping period, 5 September to 29 October 2016.

2.2.3. IFSAR DEM

The 5 m IFSAR DEM in 2014 (<http://viewer.nationalmap.gov/basic/> access date: December 2018) is currently the best available DEM for the study region with an accuracy of 0.53 ± 1.38 m (mean \pm 1 standard deviation) relative to ICESat (Yang et al., 2020). We resampled the DEM to 30 m resolution, and used it as topography reference for image coregistration, geocoding, and topographical correction.

3. Method

We applied SAR offset tracking using 93 Sentinel-1 images to derive 92 surface speed fields (79 of them with >90% spatial coverage, Table S3 in Supporting Information S2, Figure S1 in Supporting Information S1) on a 90×90 m grid for all glaciers on the Kenai Peninsula between 22 October 2014 and 13 December 2019.

3.1. Offset Tracking

Offset tracking is widely used in glacier motion assessment, using patch cross-correlation optimization of intensity images. This technique provides an alternative to DInSAR, which is limited by decorrelation in regions of rapid and incoherent flow (Kumar et al., 2013; Michel & Rignot, 1999; Strozzi et al., 2002). We applied intensity

offset tracking on a set of SAR image pairs of repeat orbits to generate offset fields through patch intensity cross correlation of SAR intensity images (Strozzi et al., 2002). The offset tracking procedure was implemented in both slant range and azimuth direction using the GAMMA® Remote sensing software in order to retrieve 2D displacement maps under the surface parallel flow assumption (Wegmüller et al., 2016).

The intensity offset tracking algorithm incorporates three main steps:

1. *Coregistration*: Images were organized in pairs in which the earlier acquired image acts as the reference image and the other as the secondary image (Table S3 in Supporting Information S2). Based on the orbit geometry and IFSAR DEM, we then calculated a coregistration lookup table for each SAR image pair. To avoid uncompensated image offsets which might completely mask out the investigated displacement (Casu et al., 2011), it is necessary to use matching techniques and spectral diversity methods (Wegmüller et al., 2016) to refine the coregistration lookup table (Sansosti et al., 2006). Furthermore, to improve the refinement procedure performance we masked out incoherence areas as well as regions with significant azimuth displacements (such as glaciers and ocean). With the automatic iterative refinements, the final coregistration was on the order of 1/1,000 of a 20 m azimuth pixel for S1 IW SLC data (1/10 of a 3 m pixel for TerraSAR-X images) and no phase jumps were visible.
2. *Offset tracking*: The azimuth phase ramp for each TOPS-mode data was deramped with an oversampling factor of two. Based on the expected maximum ice displacements and results from previous studies (Baurley et al., 2020; Dall et al., 2015; Sánchez-Gámez & Navarro, 2017), for the Sentinel-1 data, we applied a patch window size of 256×128 single-look pixels in the range and azimuth directions and a step size of 40×8 pixels in the offset tracking procedure, while for TerraSAR-X we used a window size of 512×512 pixels and 32×32 pixels for the step size. We discard pixels with unreliable offset values by the signal-to-noise ratio threshold of 6.0, which is defined as the ratio of the cross-correlation function peak to the average correlation on the tracking window (Strozzi et al., 2002).
3. *Geocoding*: The offset maps were geocoded using the IFSAR DEM and SAR imaging geometry, and then gridded on the 90×90 m grid, transformed to UTM-6N, based upon the WGS84 ellipsoid. Finally, a median low-pass filter (3×3 pixels) was used to eliminate individual outliers, and we manually checked for blunders in the automatic results and applied corrections where necessary (Heid & Kääb, 2012; Paul et al., 2015).

3.2. Uncertainty Analysis

Uncertainties in surface velocity arise primarily from inexact coregistration of the SAR images (σ_{coreg}), errors in the intensity-offset tracking algorithm (σ_{track}) (McNabb et al., 2012; Seehaus et al., 2015), and the ionospheric effect (σ_{iono}) (Gray et al., 2000). Assuming all errors are independent of each other, we estimated the total error (σ) by

$$\sigma = \sqrt{\sigma_{\text{coreg}}^2 + \sigma_{\text{track}}^2 + \sigma_{\text{iono}}^2} \quad (1)$$

The uncertainty for each image pair is given in Table S3 in Supporting Information S2, and the averaged error is $0.19 \pm 0.06 \text{ m d}^{-1}$ (ranging from 0.06 to 0.28 m d^{-1}). σ_{coreg} is derived from the offset values on stable terrain (terrain without glaciers, water, and vegetation). Since σ_{coreg} is not normally distributed (Figure S2 in Supporting Information S1), we describe the error in terms of the median and the normalized median absolute deviation, which is a robust alternative to the standard deviation (Rousseeuw & Croux, 1993). The average value is $0.06 \pm 0.03 \text{ m d}^{-1}$. σ_{track} is estimated by

$$\sigma_{\text{track}} = \frac{C \Delta x}{z \Delta t} \quad (2)$$

where C is the uncertainty of the offset tracking algorithm in number of pixels (here assumed to be 0.4; Seehaus et al., 2015; Vijay & Braun, 2017); Δx is the SAR image resolution in ground range geometry (14 and 2.5 m for Sentinel-1 and TerraSAR-X data, respectively); z is the applied oversampling factor for Sentinel-1 images (here $z = 2$); and Δt is the repeat interval between image pair acquisitions (12, 24, 36, 48, or 54 days for Sentinel-1 and 11 days for TerraSAR-X; Table S3 in Supporting Information S2). The average value of σ_{track} is 0.17 m d^{-1} .

σ_{iono} , the azimuth offset error between a repeat orbit SAR image pair (Wegmüller et al., 2016), is introduced by ionospheric anomalies. Varying significantly with time, position, and the wavelength of the radar sensor, it is difficult to quantify precisely. As confirmed in many studies, ionospheric disturbances are much stronger in L-band than C- and X-band radars, and more abundant near the magnetic pole (Joughin et al., 2010). For the Sentinel-1 TOPS IW mode data sets (C-band), we used a high-pass filter along the range direction to reduce the streaks (Wegmüller et al., 2006) and estimated $\sigma_{\text{iono}} = 0.02 \text{ m d}^{-1}$ (following Nagler et al. (2015)). For the TerraSAR-X data we assumed that σ_{iono} is negligible due to the higher frequency system, better resolution, and higher sensitivity to deformation, as well as lower susceptibility to ionospheric disturbances (Brcic et al., 2011; Paul et al., 2017; Wegmüller et al., 2006).

In addition, geocoding can introduce uncertainty, mainly caused by the DEM error (Nagler et al., 2015). Since geocoding was performed independently for each displacement field after offset derivation, and the relative height between neighboring DEM pixels is much more important than the absolute height in the process (Luckman et al., 2007), the DEM artifacts do not propagate and have little or no effect on the final velocity map (E. Burgess et al., 2012). Some studies have reported a bias of 0.5% and 0.8% over a period of 8 years for the Greenland and Antarctic Peninsula, respectively (Nagler et al., 2015; Rohner et al., 2019; Seehaus et al., 2015). In this study, lacking an updated DEM, we do not account for the effect of surface lowering on the slant range displacement and assume it to be negligible. Further error contributions related to atmospheric water vapor as well as the tidal influences for the tidewater glacier are still difficult to quantify and thus neglected.

3.3. Evaluation

Lacking in situ measurements, we evaluate the accuracy of the Sentinel-1-derived ice speeds by comparing them to those derived from TerraSAR-X images by intensity offset tracking as done in previous studies (Lemos et al., 2018). Speeds were compared pixel by pixel only for the TerraSAR-X image pair accessible in this domain acquired on 23 September and 4 October 2016. The closest available Sentinel image pair is from 5 September and 29 October 2016, with a 11-day overlap.

Results for Bear Glacier are shown in Figure 2. Sentinel-1 results agree well with the TerraSAR-X ice speeds in most parts of the main branch of the glacier with absolute differences less than 20 m a^{-1} ; however, differences exceed 100 m a^{-1} in the fastest flowing parts. On average, the TerraSAR-X speeds are larger than the Sentinel-1 speeds, with a mean difference of 8.6 m a^{-1} (corresponding to 11% of the mean speed derived from TerraSAR-X), median value of 4.2 m a^{-1} , and a standard deviation of 43 m a^{-1} (Figure 2c). We attribute part of the discrepancy to the longer period spanned by the Sentinel image pair (54 days vs. 11 days).

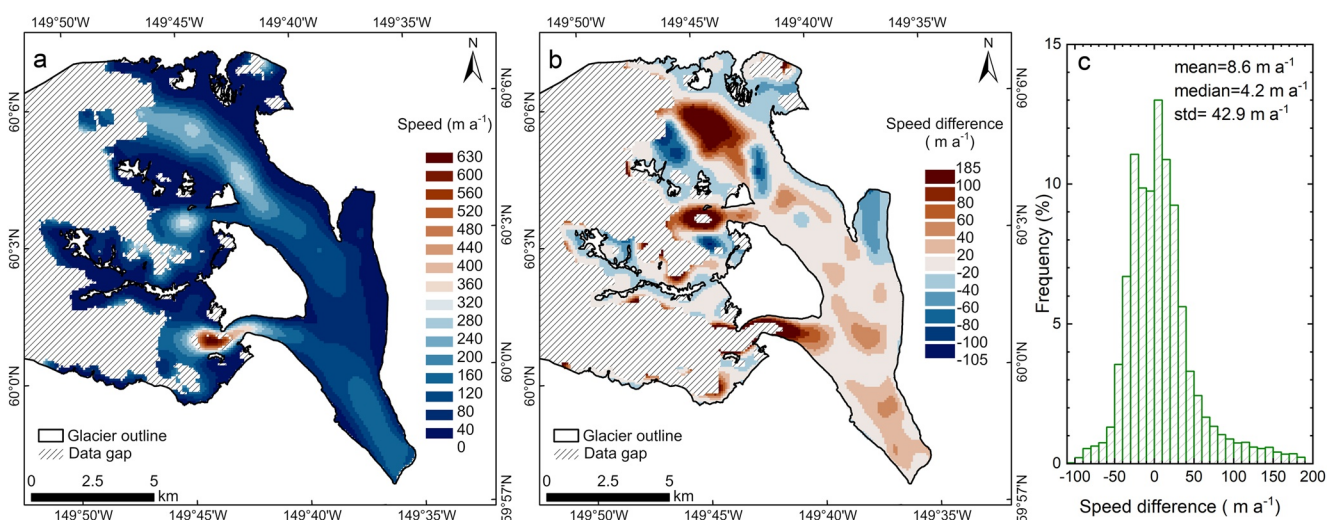


Figure 2. Evaluation of Sentinel-1-derived glacier surface speeds using TerraSAR-X-derived speeds over Bear Glacier. (a) TerraSAR-X-derived ice speeds over the period 23 September to 4 October 2016. (b) Differences in ice speed (TerraSAR-X minus Sentinel-1). Hatched white areas in panels (a) and (b) mark data gaps. (c) Histograms of the values in panel (b) with a bin size of 10 m a^{-1} .

3.4. Time-Averaged Ice Speed Mapping

Annual and seasonal surface ice speed fields were generated from the error-weighted average of all ice speed fields within the considered averaging period following Joughin et al. (2018). The weights were calculated from $1/\sigma^2$, where σ is the precision of each ice surface speed field for each image pair as listed in Table S3 in Supporting Information S2, and then normalized such that they sum up to 1. In addition, we weighted each pair's speed by its duration of overlap with the considered period. For each pixel, we computed the error-weighted average only when the temporal coverage was greater than 70% and considered the remaining pixels as data gaps ($\sim 5\%$ of the total glacier area).

The uncertainty of the temporal-averaged ice speed fields (σ_m) was estimated by propagating the error of each field in the period considered:

$$\sigma_m^2 = \frac{1}{\sum_{i=1}^N \left(\frac{1}{\sigma_i^2} \right)} \quad (3)$$

where σ_i is the uncertainty of each individual speed field (Table S3 in Supporting Information S2) and N is the number of samples contributing to the weighted average.

4. Results

4.1. Spatial Ice Speed Patterns

Glacier mean surface speed over the 5-year period varies between 9 and 600 m a⁻¹ across the study area with the fastest flow occurring in the lower reaches of the Aialik and Chenega glaciers, which both are tidewater glaciers (Figure 3). Approximately 90% of the glacierized surface across the Kenai Peninsula has a mean speed less than 160 m a⁻¹ and 70% flows at mean speeds less than 80 m a⁻¹. The average glacier speed for the whole region is 69 m a⁻¹ (the median is 51 m a⁻¹) with an uncertainty $\sigma_m = 6.5 \pm 0.7$ m a⁻¹ ($\sim 10\%$). Ice flow speeds were generally higher on the coastal side (east) where the tidewater glaciers and several lake-terminating glaciers are located than those on the inland side (west).

4.2. Ice Speed Variations Along Glacier Centerlines

Ice speed patterns along longitudinal profiles vary widely between glaciers depending on local morphology and glacier characteristics; however, we find distinct patterns related to terminus type. A typical example of ice speed variations along the glacier centerline is shown in Figure 4 for each terminus type, and median profiles are shown in Figure 5. As expected, land-terminating glaciers have their speed maxima around the median elevation which is often close to the balanced-budget Equilibrium-Line Altitude (ELA₀; Braithwaite & Raper, 2009). There, the glacier tends to be thickest, and the largest ice volume needs to be passed through for the glacier to keep or reach a steady state. The tidewater glaciers have their speed maxima close to the terminus consistent with other studies elsewhere (McNabb et al., 2012; Meier & Post, 1987; Rohner et al., 2019; Sakakibara & Sugiyama, 2018; Vallot et al., 2017; Vieli et al., 2004). Like land-terminating glaciers, most lake-terminating glaciers have their minimum speeds at the highest and lowest glacier elevations, however, the location of the speed maximum along the centerline exhibits more variation.

4.3. Seasonal Ice Speed Variations

To investigate seasonal variations, we computed a seasonal enhancement factor defined as the ratio of 3-month averaged speeds and the mean speed over the 5-year period December 2014 to November 2019 (Figure 6). The factor quantifies for each pixel how much in each season the speeds are higher or lower than the pixel's annual mean, with the average value 1 and the error level of 0.1. Most strikingly, the spring speeds are equal or greater than the annual mean almost everywhere. On average, speeds are 50% greater than the annual mean. In all other seasons some areas show greater and others smaller speeds than the annual mean but overall maximum deviations to the mean are smaller than in spring. Summer and fall speeds are on average 86% and 87% of the annual mean, respectively. On average, winter speeds are close to the annual mean (96%) and thus provide a good

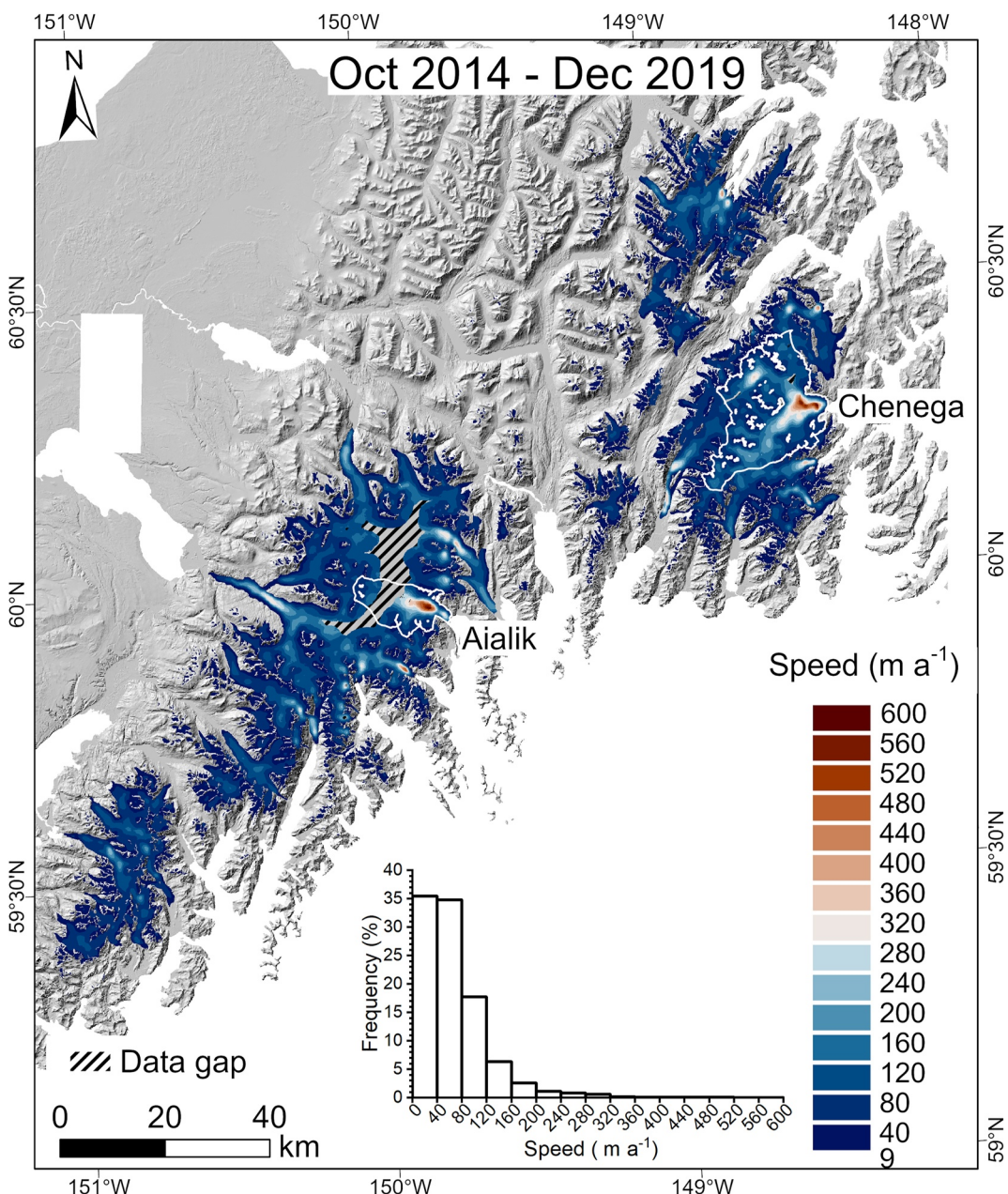


Figure 3. Spatial distribution of surface speed averaged over the period October 2014 to December 2019 and histogram of speed distribution. Data gap on the Harding Icefield occurs because the offset tracking algorithm performed poorly due to low image contrast. The two glaciers with the highest speeds are outlined and named.

approximation of annual mean speeds consistent with findings in other regions in Alaska (Burgess et al., 2013; McNabb et al., 2015).

To investigate differences in ice speed seasonality between terminus types, we calculated a monthly enhancement factor for individual glaciers defined as the ratio of each glacier's monthly mean and annual mean ice speed over the period December 2014 to November 2019. We selected all 77 glaciers $>3 \text{ km}^2$ that are connected to any of the large icefields (Figure S3 in Supporting Information S1) including 48 land-terminating glaciers, 18 lake-terminating glaciers, and 11 tidewater glaciers. We computed the monthly enhancement factor for two locations on each glacier: (a) a site close to the terminus defined by a $270 \text{ m} \times 270 \text{ m}$ square around the point on the centerline that is at one-tenth the total length of the glacier centerline up-glacier from the terminus, and (b) a site around the

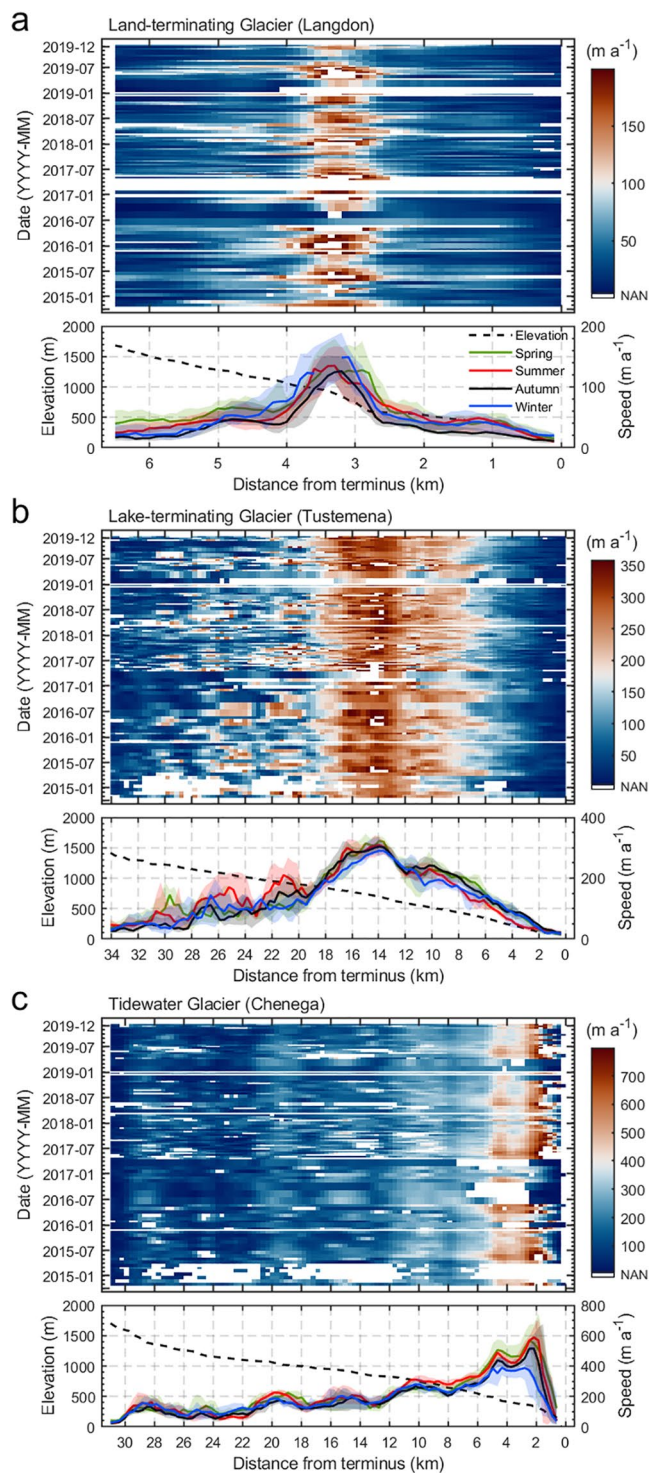


Figure 4. Temporal evolution of surface speed profiles of selected glaciers with different terminal types. Speeds are averaged over 180×180 m windows along the centerline. Data are shown for all 92 image pairs separated by 12–54 days (Table S3 in Supporting Information S2) between October 2014 to December 2019 (upper panels) and the median speed with the interquartile range (IQR) over spring (MAM), summer (JJA), fall (SON), and winter (DJF, lower panels). Data gaps in the upper panels are shown in white. The x-axis refers to the distance from the terminus in Oct 2014. Terminus positions were relatively stable in panels (a) and (b), while Chenega Glacier (c) retreated ~ 300 m over the study period. Elevation data along the centerlines are from the IFSAR DEM. Note the speed scale is different between the subplots.

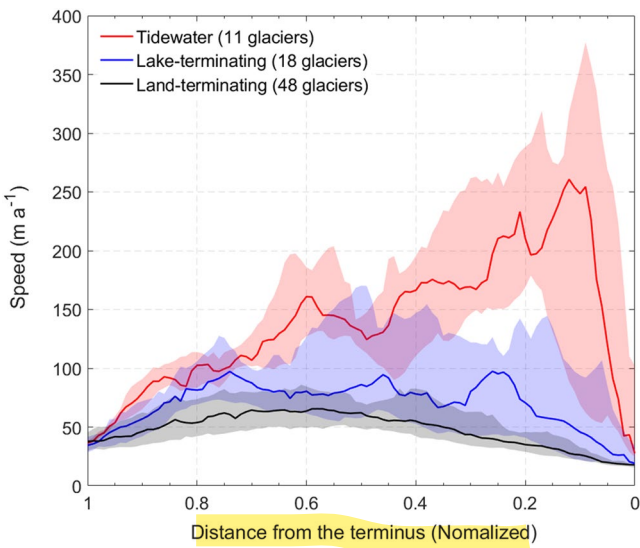


Figure 5. Surface speed profiles along the glacier centerline for different terminus types. Median and the interquartile range calculated in bins of 0.01 are shown for each glacier type. The distance from the terminus is normalized by the centerline length for each glacier.

median glacier elevation along the centerline and therefore close to the ELA₀ (Braithwaite & Raper, 2009, Figure 7). Despite large variations between individual glaciers, a coherent seasonal pattern is obvious for both sites regardless of terminus type (Figure 7). Ice flow exhibits a significant spring speedup typically reaching a peak in May, followed by a slowdown during summer and early fall reaching a minimum in September/October. A secondary peak, less pronounced than the spring peak, is reached in November, and in winter speeds are close to the annual mean consistent with Figure 6. While the overall pattern is similar for all glacier types, land-terminating glaciers tend to experience more pronounced seasonal amplitudes than the tidewater and lake-terminating glaciers, although we note that interquartile ranges overlap in most months and sample sizes vary between the three glacier types (Figure 5).

4.4. Interannual Variations

We computed annual mean surface speed maps for each calendar year from 2015 to 2019 revealing no significant interannual variation in the spatial pattern (Figure S4 in Supporting Information S1). To further examine the interannual changes and flow characteristics for glaciers with different terminus types, we also analyzed the time series of the pixel-averaged monthly speeds of land-terminating, lake-terminating, and tidewater glaciers (Figure 8). Monthly variations over the 5-year period are largely synchronous among the three glacier types. In addition, annual mean speeds remained relatively stable with an interannual variability of $\pm 10\%$ of the period mean, consistent with findings on the Juneau Icefield, Alaska, between 1995 and 2011 (Melkonian et al., 2014), and Taku Glacier, Alaska, during 1950–2006 (M. S. Pelto et al., 2008). Figure 8 also indicates that the tidewater glaciers tend to flow considerably faster than the lake-terminating glaciers, which in turn are faster than the land-terminating glaciers.

5. Discussion

5.1. Seasonal Variation

Our observed seasonal flow speed variations with distinct speed-up in spring followed by a gradual slow-down over summer are consistent with observations on many other glaciers for example, Columbia glacier (Vijay & Braun, 2017) and Hubbard glacier (Trabant et al., 2003) in Alaska, as well as glaciers in Greenland (Davison et al., 2020; Moon et al., 2014; Vijay et al., 2019) and Svalbard (Schellenberger et al., 2015). These seasonal variations are associated with changes in basal motion as meltwater input varies and the subglacial drainage system evolves from an inefficient distributed drainage system to a channelized system during the melt season (Kamb, 1987; Röthlisberger, 1972; Walder, 1986). Increased meltwater input at the onset of the melt season will lead to increased water pressure and reduced basal drag, and thus a speedup. As an efficient channelized subglacial drainage system evolves during summer capable of accommodating large amounts of melt water, the glacier gradually slows down until the system reverts to a distributed system as meltwater input is reduced. The observed secondary peak in early winter, similar to findings in Svalbard (Schellenberger et al., 2015) and Bench Glacier, Alaska (Fudge et al., 2009), is attributed to high precipitation rates in fall allowing large quantities of water to enter the drainage system despite declining melt at this time of year (Figure 9).

5.2. Flow Speed Variations for Different Terminus-Type Glaciers

There are distinct differences between ice speeds and their spatiotemporal variations between glaciers of different terminus types, but also synchronous behavior. Longitudinal flow speed profiles differ strongly (Figures 4 and 5). The tidewater glaciers' speed maximum close to the terminus is consistent with observations elsewhere (e.g., Svalbard (Vieli et al., 2004) and Alaska (McNabb et al., 2012; O'Neil et al., 2001)), and can be attributed to

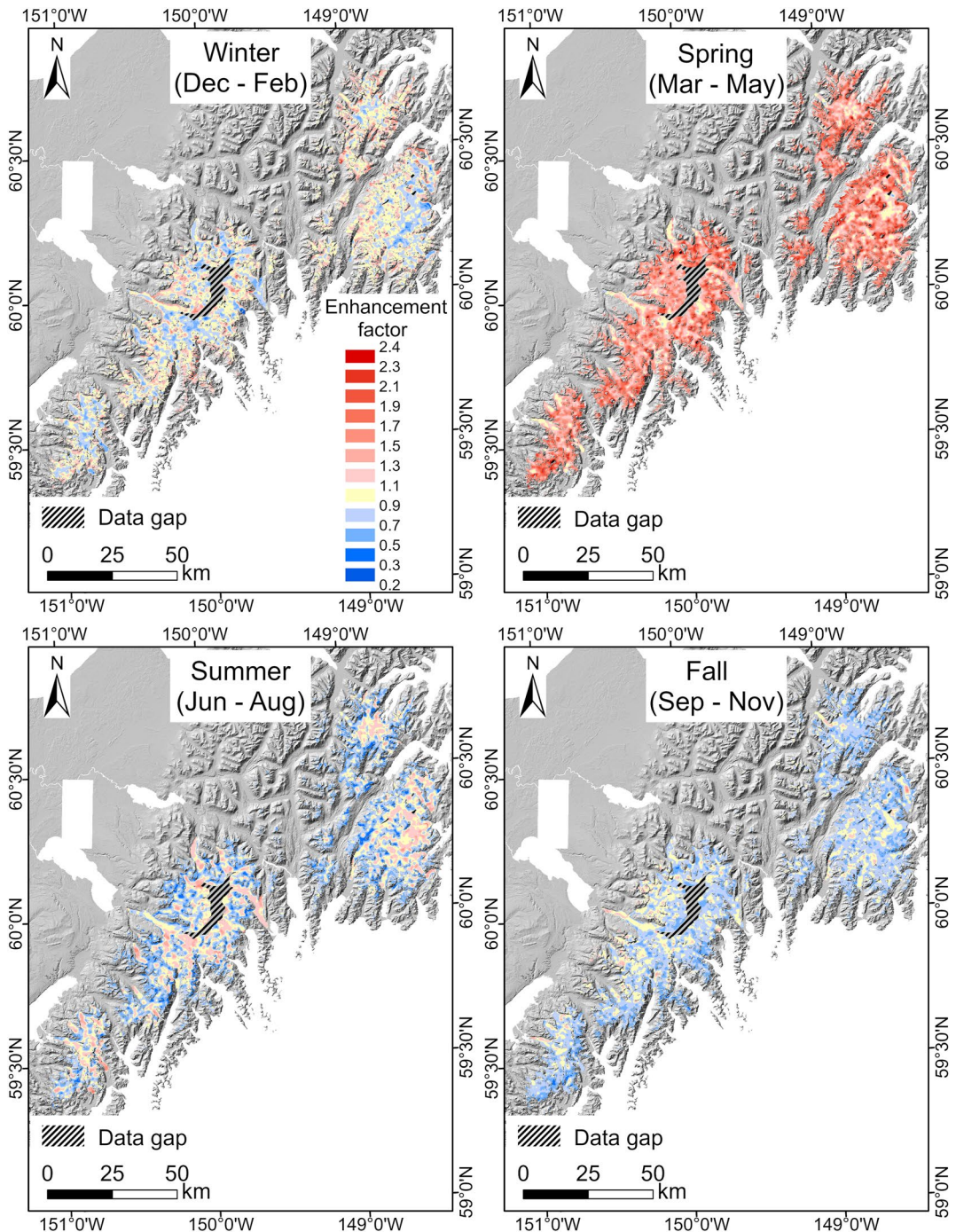


Figure 6. Seasonal enhancement factor maps indicating the deviation of seasonal glacier surface speeds relative to each pixel's annual mean. The enhancement factor is defined as the ratio of seasonal (3 months) and 5-year mean ice speeds averaged over the period December 2014 to November 2019.

ice-ocean interactions depending on tidal forcing and ocean temperature. Ogive Glacier and Anchor Glacier are exceptions, with speed maxima near their median elevation. Repeat photography comparison from Kenai Fjords National Park's Service (NPS) shows that both glaciers have rapidly retreated and thinned at their termini the last 30 years (<https://www.nps.gov/kefj/learn/nature/glacier-repeat-photography.htm>). Most lake-terminating glaciers tend to have their maximum closer to the median elevation, as typical for land-terminating glaciers. This suggests these glaciers experience relatively little mass loss due to frontal ablation, and thus the lakes' impact on terminus

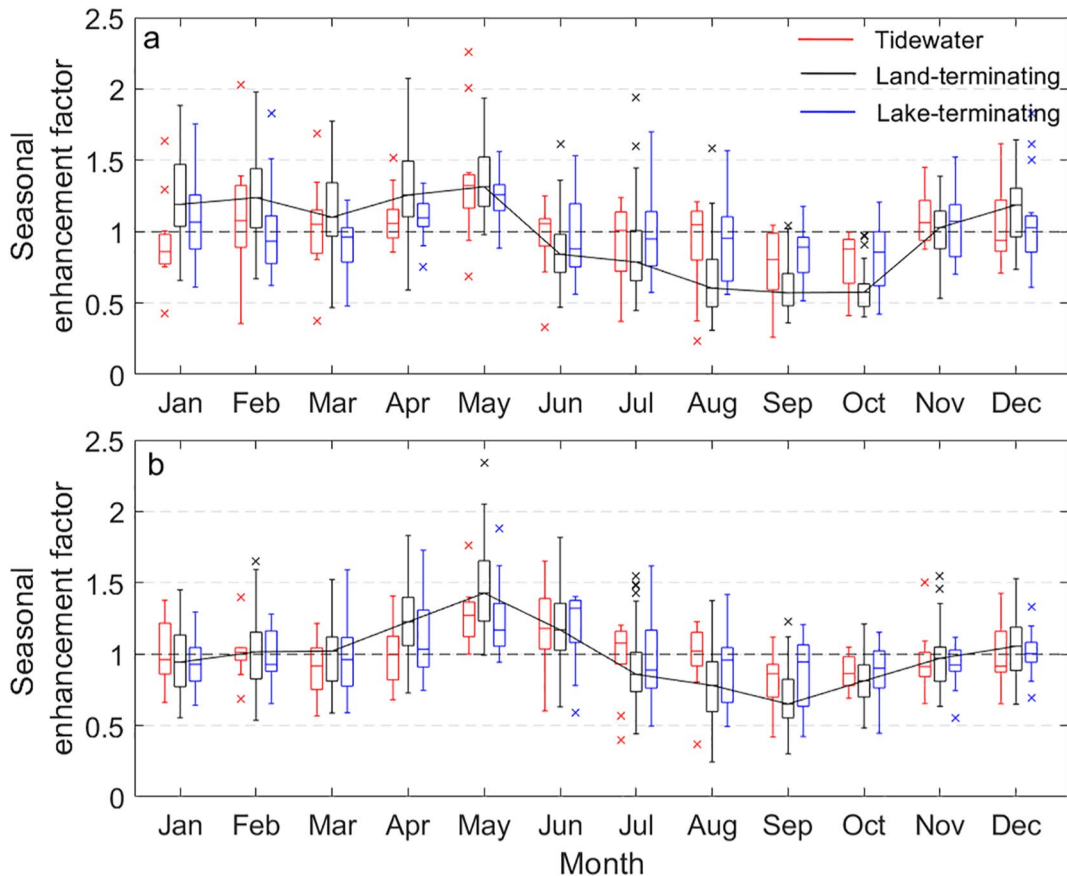


Figure 7. Boxplot showing the monthly averaged enhancement factors of surface speed for two sites for 77 glaciers. The enhancement factor is shown for all glaciers that are larger than 3 km^2 and originate from any of the larger icefields, including 48 land-terminating, 18 lake-terminating, and 11 tidewater glaciers (Figure S3 in Supporting Information S1). (a) A point near the terminus and (b) a point near the median elevation along the centerline are shown. Outliers are plotted as crosses (defined as all values 1.5 times the interquartile range larger [smaller] than the third [first] quartile). The black line connects the monthly median (only shown for land-terminating glaciers for better readability).

speed is negligible. This is consistent with findings at other lake-terminating glaciers where in contrast to tidewater glaciers frontal ablation has been found to play a minor role (Truffer & Motyka, 2016), except temporarily in cases of rapid terminus collapse such as observed at Yakutat Glacier, Alaska (Trüssel et al., 2013). However, three lake-terminating glaciers in this region have their maximum speed near the terminus (Bear Glacier and Ellsworth Glacier [further discussed in Section 5] and Excelsior Glacier).

While land-terminating glaciers flow at a speed of $\sim 43 \text{ m a}^{-1}$ on average over the period October 2014 to December 2019, lake-terminating and tidewater glaciers flow 1.7 times and 2.3 times faster, respectively. Part of the differences can be attributed to differences in glacier size (and associated thickness). Although on average half as steep as the 1,431 land-terminating glaciers, the 18 lake-, and 11 marine-terminating glaciers are almost two orders of magnitude larger (Yang et al., 2020) and thus considerably thicker (Farinotti et al., 2019). The greater flow speeds of the tidewater glaciers compared to the other two types can be attributed to additional mass losses due to frontal ablation (iceberg calving and submarine melt) at the calving front (most likely exceeding those of the lake-terminating glaciers considerably; Truffer and Motyka (2016)) and larger mass turnover due to greater snow accumulation and steeper mass balance gradients close to the coast where these glaciers are located compared to western inland locations (E. W. Burgess et al., 2013).

On the other hand, the three glacier terminus types show similar behavior with respect to short-term temporal variations (Figure 8a). The amplitude of the tidewater glacier monthly speed anomalies is greater than that for the lake-terminating glaciers followed by the land-terminating glaciers (Figure 8b) consistent with the differences in

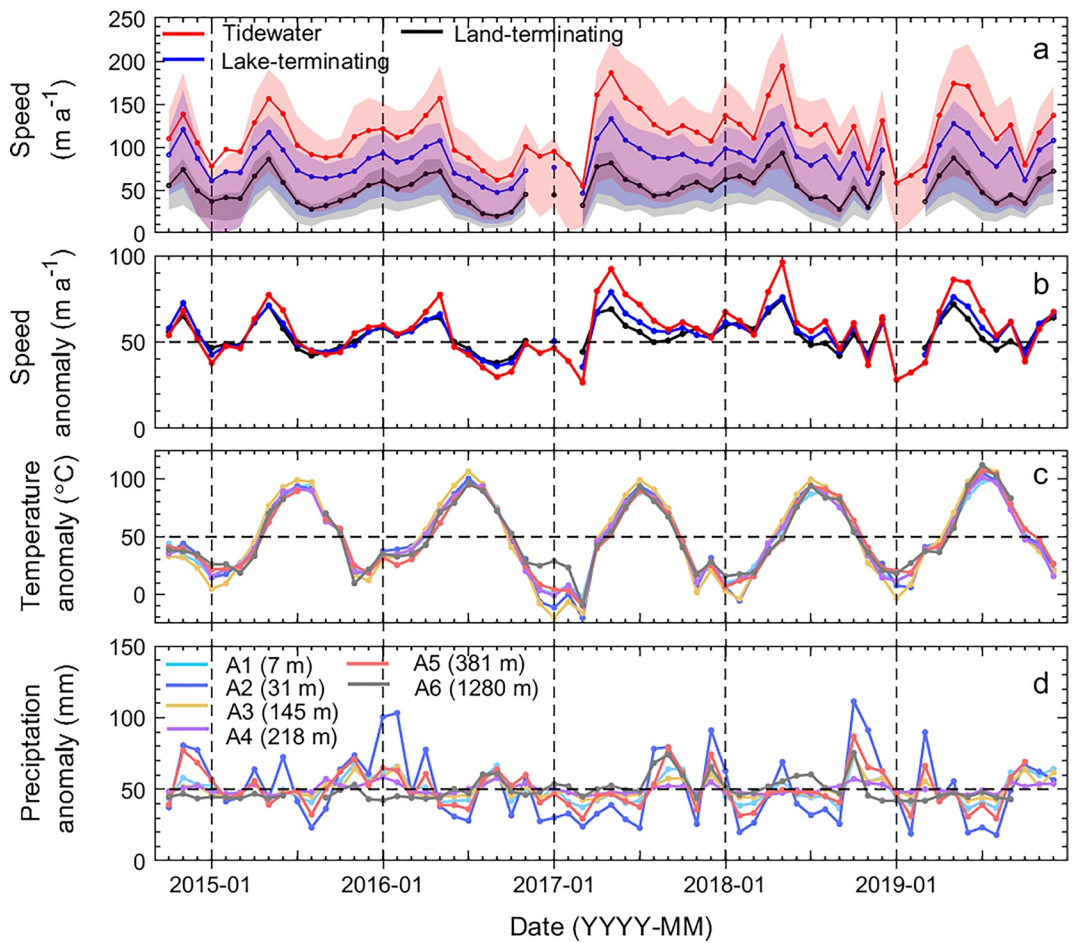


Figure 8. Time series of monthly ice surface speeds and meteorological data during the period October 2014 to December 2019. (a) Monthly mean speeds averaged over all land-terminating, lake-terminating, and tidewater glacier pixels, and the interquartile range (filled area). (b) Monthly speed anomalies relative to the period means shown in panel (a). (c, d) Anomalies for monthly mean temperature and monthly total precipitation at the weather stations A1–A6, relative to the period mean (Figure 1, Table S2 in Supporting Information S2; data from A7, A8, and A9 are not plotted for better visibility since they have similar elevations as the stations shown). Gaps are present where the monthly temporal coverage is <70%.

average ice speeds (Figure 8a). However, monthly speedups and slowdowns occur simultaneously regardless of the terminus type. This behavior cannot be explained by errors in the processing chain because the image pairs could be successfully coregistered with no visible phase jumps. This synchronous behavior suggests that the monthly speed variations are controlled by regional-scale meteorological drivers governing the water input to the drainage system across the entire peninsula. We found no correlation between annual mean speed and summer precipitation averaged over six weather stations but a weak though significant negative correlation with summer air temperature, indicating a slowdown with presumably more meltwater due to a warmer summer (Figure S5 in Supporting Information S1). However, caution should be taken interpreting these results since the time series is short (5 years) and it remains unclear how representative the weather stations are for the conditions on the glaciers. Most importantly a mass-balance model is needed to compute total water input to the system from both melt and rainwater to examine the relation between speed and water input.

Seasonal variations are also similar between terminus types indicating that variations in seasonal melt and rainwater input are the dominant driver in the observed seasonal speed variations. However, the amplitudes at two examined points on the glaciers are somewhat larger for the land-terminating glaciers than the other two types. While the seasonal speed changes of land-terminating glaciers are largely dependent on the changes in subglacial hydrology (Moon et al., 2015), the water-terminating glaciers are also influenced by the ocean/lake water acting to smoothen out the seasonal variations.

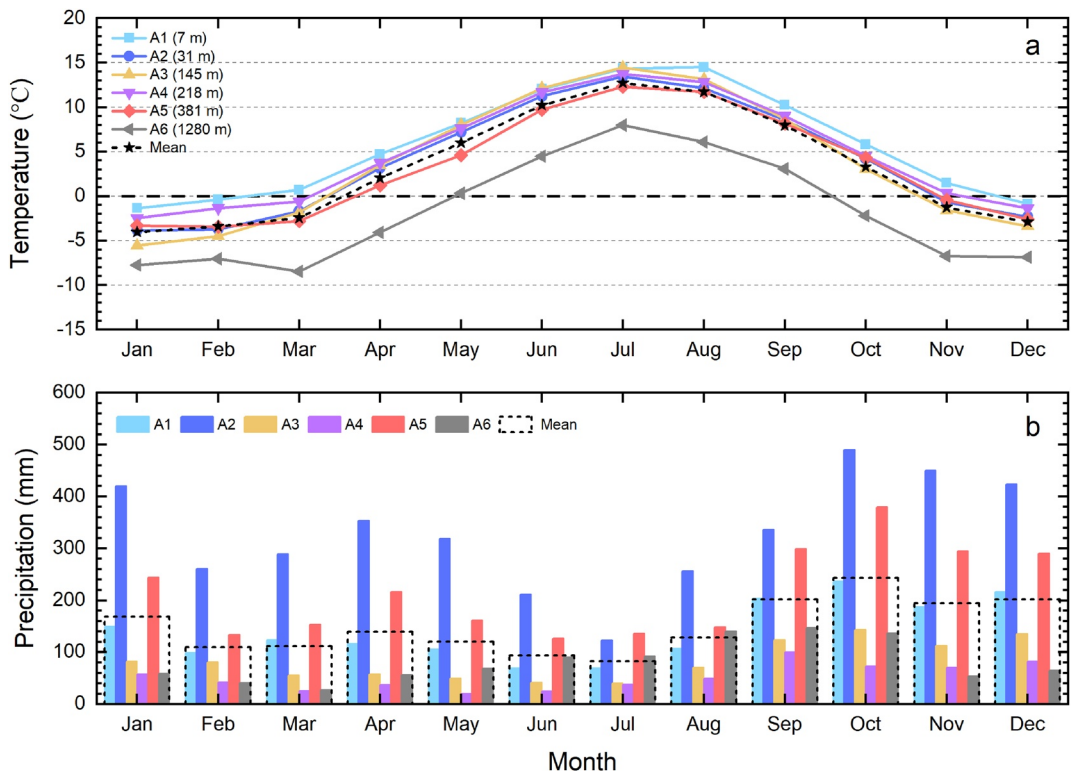


Figure 9. Monthly mean air temperature and precipitation data from six weather stations on the Kenai Peninsula (Figure 1) averaged over the period October 2014 to December 2019.

5.3. Speed Variations and GLOFs

Near-annual GLOFs have been observed at Bear glacier, the longest (~35 km) and largest (202 km^2) lake-terminating glacier on the Kenai Peninsula often causing flooding events in the proglacial lake at the terminus (~ 19 km^2 in 2019; Lanik et al., 2018; Wilcox et al., 2014). The GLOFs originate from an ice-dammed lake with a lake area of ~0.35–0.5 km^2 (Wilcox et al., 2014), ~11 km up-glacier from the terminus, which forms at the front of a smaller ice lobe spilling into an ice-free tributary valley (Figure 10a). A time lapse camera installed in June 2017 by the Kenai Fjords NPS recorded the onset and duration of two GLOFs that occurred in 2018 (5–15 August) and 2019 (3–9 September), and thus during our study period.

To investigate the impact of these events on ice motion we calculated the time series of the pixel-averaged flow speed of the area above and below the lake roughly defined by the 400 m contour line (Figure 11). During the GLOF in 2019 the area below the ice-dammed lake accelerated strongly, reaching speeds roughly three times the average flow speed of the entire study period, before dropping rapidly to pre-GLOF values. The image pair that includes the 6-day duration of the GLOF is separated by 24 days (27 August to 20 September) suggesting that the actual flow acceleration during the GLOF was much larger. The area above the 400 m contour line also accelerated probably due to longitudinal coupling; however, the speedup was considerably smaller, clearly indicating that the GLOF is responsible for the flow acceleration of the lower part. Also, no unusual temperature or precipitation events were recorded at a nearby weather station during the GLOF (Figure 11). The acceleration is consistent with the notion that the draining lake water is overwhelming the subglacial drainage system forcing water out of subglacial channels into neighboring hydraulically less efficient areas, thus lubricating the bed and weakening the coupling of the glacier with its bed (Bartholomaus et al., 2008; Iken & Bindschadler, 1986; Iken et al., 1983). Flow speed accelerations of two to fourfold the pre-GLOF rates over parts of a glacier affected by the drained water have also been observed on glaciers in Iceland (Magnússon et al., 2007) and central Asia (Neelmeijer et al., 2014).

In contrast, the Bear Glacier GLOF in 2018 had a negligible impact on flow speed although the ice speed averaging period given by the available image pair (8–20 August) is only slightly longer than the duration of the GLOF

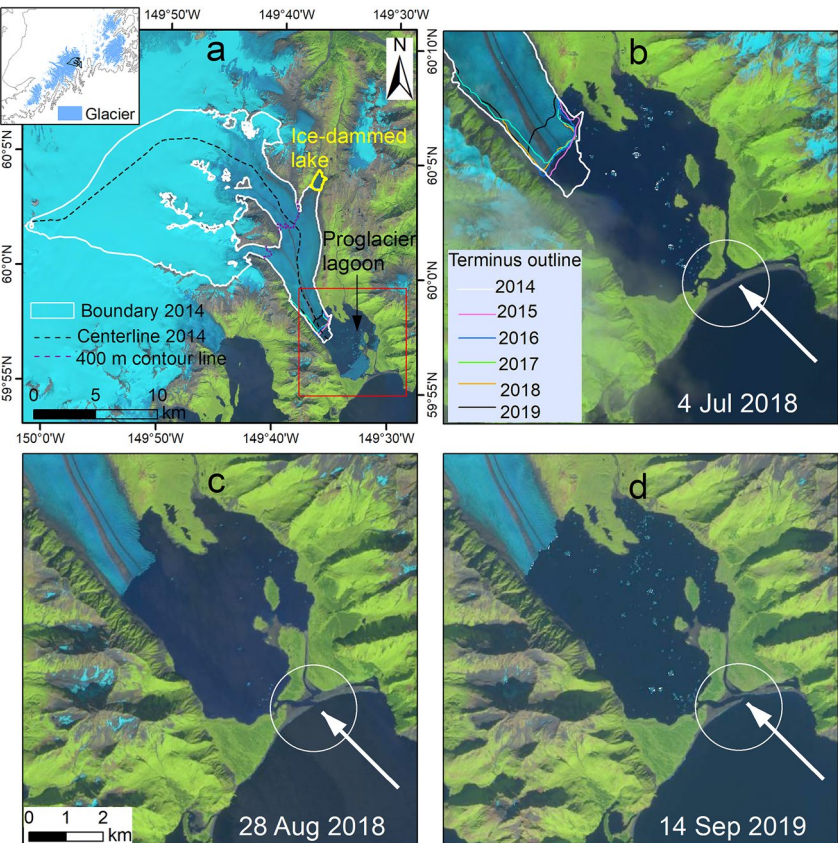


Figure 10. Sentinel-2 images showing morphological changes between the lagoon in front of Bear Glacier and the ocean between July 2018 and September 2019. Glacier lake outburst floods (GLOFs) occurred during 7–15 August 2018 and 3–9 September 2019. Dates refer to the acquisition dates of the Sentinel-2 images. The arrow marks the location where the beach barrier between the lagoon and ocean was breached after the August 2018 GLOF. The red square in (a) depicts the area shown in (b)–(d).

(7–15 August). Possibly the subglacial channelized drainage system was sufficiently developed and lake volumes smaller so that the drainage system could accommodate the additional water input due to the GLOF.

Although not causing an immediate short-term ice speed response, the GLOF in 2018 seems to be the trigger for a longer-term speed-up of the glacier in the terminus area. Figure 12 shows that seasonal ice speed variations along the centerline remained relatively stable from year to year except for the lowest ~8 km from the terminus where the flow accelerated in 2019 by >60% compared to the average over the preceding years. Thus, the centerline speed profile typical of the most lake-terminating glaciers in this region with a pronounced flow maxima around the median altitude changed to a profile with two distinct speed maxima. The acceleration is notable in all seasons although less pronounced in winter (Figure 12b).

Observations from airplanes indicated that the low-lying moraine barrier separating Bear Glacier Lake and the ocean was breached during the GLOF probably in response to the resulting increase in lake level by roughly 2 m (Kurtz & Wolken, 2019). A similar breach was observed in response to the GLOF in August 2014 but then the barrier was naturally repaired within the following months. In contrast, the moraine breach in August 2018 persisted at least throughout 2019 as evident from Sentinel-2 images (Figure 10), subjecting the lake to the inflow of ocean water as well as tidal and wave activity. Airplane observations confirmed such inflow of ocean water (Kurtz, D., personal communication, 2021). This may have triggered a density-driven circulation typical of tidewater glacier proglacial environments causing enhanced subaqueous melt and calving rates and thus retreat and thinning consistent with observations. The glacier retreated about 1.1 km within 1 year following the GLOF in August 2018 after largely stable terminus positions during the preceding years (Figure 10b) and the thinning

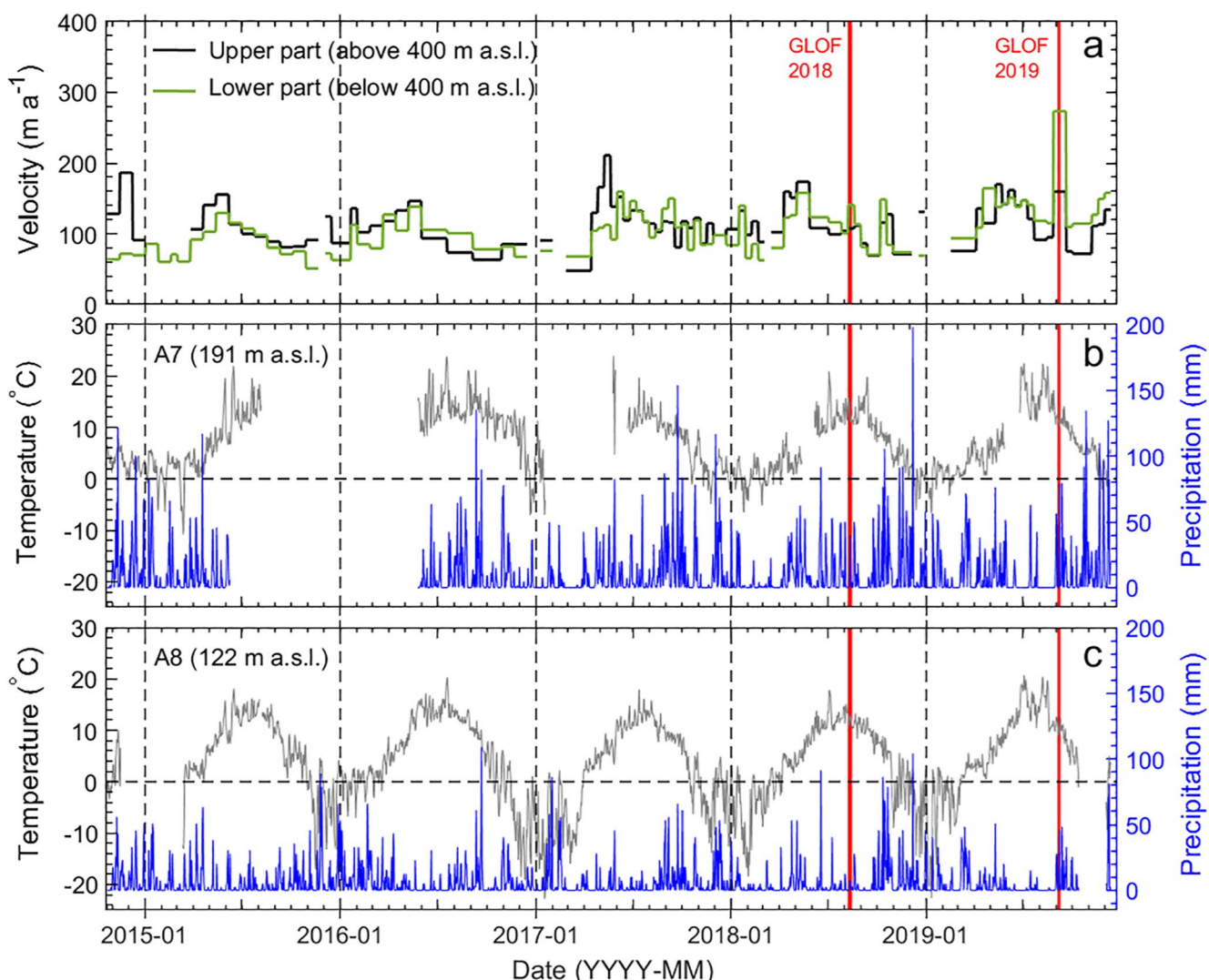


Figure 11. Time series of surface speed of Bear Glacier and meteorological data nearby between October 2014 and December 2019. (a) Pixel-averaged mean speed of the glacier area >400 m a.s.l. (only pixels with valid data) and below the drained ice-dammed lake (<400 m a.s.l.). (b, c) Monthly mean temperature and monthly precipitation at weather stations nearby weather stations A7 (b) and A8 (c) (Figure 1 and Table S2 in Supporting Information S2).

rate of the terminus region tripled in 2018/2019 compared to the previous two mass-balance years (Kurtz, D., personal communication, 2021).

Further facilitated by greater salinity it is also possible that part of the glacier terminus became buoyant thus amplifying the flow acceleration. The possibility of a floating tongue has also been suggested as a trigger of a dramatic retreat between 2000 and 2005 (Giffen et al., 2007). Similar behavior of rapid retreat, surface thinning, and flow acceleration have been widely observed on tidewater glaciers, such as Columbia glacier in Alaska (O’Neal et al., 2005) and tidewater glaciers in Greenland (Howat et al., 2007; Joughin et al., 2004, 2008) and Antarctica (Pritchard & Vaughan, 2007), but also some lake-terminating glaciers, for example, Yakutat Glacier in Alaska (Trüssel et al., 2013) and Upsala Glacier in Patagonia (Sakakibara et al., 2013). Direct observations would be needed to provide conclusive explanations for the speedup at Bear Glacier, however, it seems likely that the GLOF-induced breach of the moraine barrier and resulting changes in the proglacial lake environment further amplified by positive feedbacks triggered the observed speedup.

Inspecting Landsat images, we also detected an ice-dammed lake at Skilak Glacier that drained twice during our study period (fall 2016 and 2018; Figure S6 in Supporting Information S1). We did not find any flow acceleration associated with the lake drainage, but we note that any GLOF-related speedup may have gone undetected due to

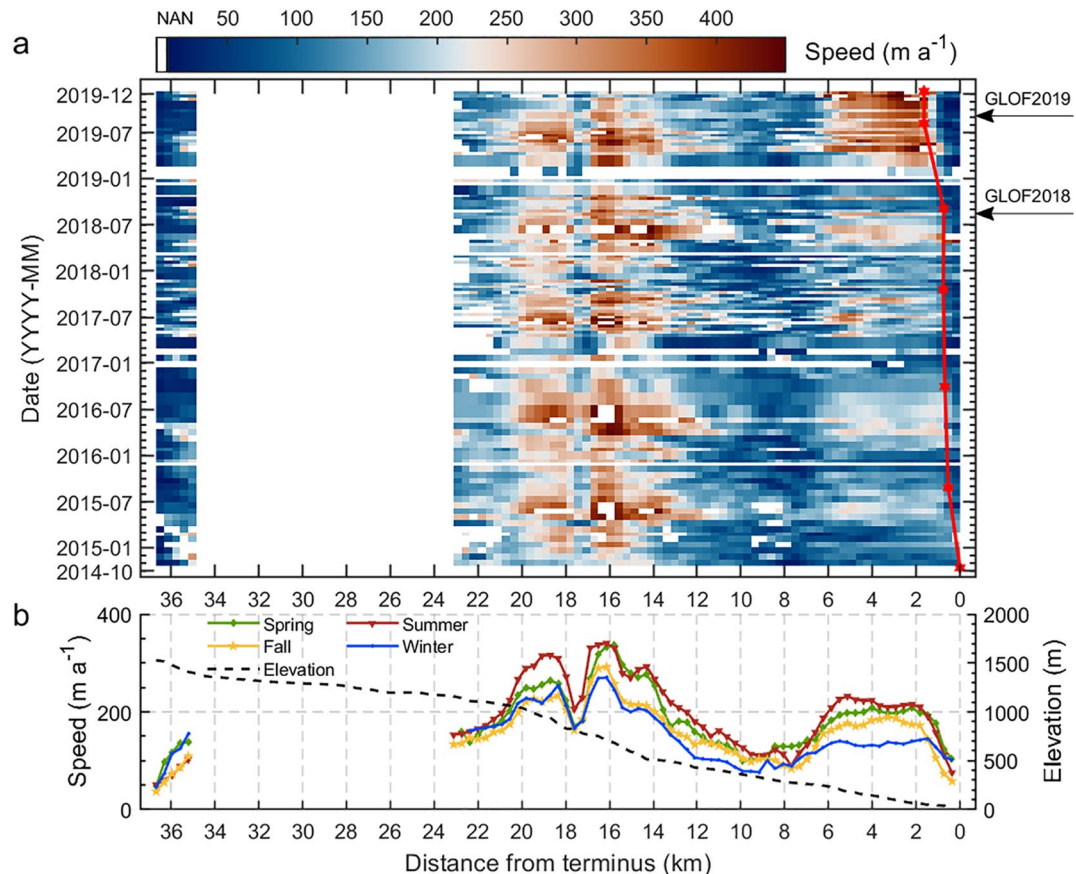


Figure 12. Temporal evolution of the surface speed profile of Bear Glacier. As in Figure 4, the speed variation on the centerline is shown in panel (a), and the averaged seasonal variations are in panel (b). The red line marks the location of the glacier terminus.

an averaging period for the ice speed calculation of 54 days for the 2016 event and 12–24 days for the 2018 event (Figure S7 in Supporting Information S1).

5.4. Terminus Variations on Ellsworth Glacier

A notable step-like speedup of the terminus region during the study period is also observed at lake-terminating Ellsworth Glacier (115 km^2 in 2014; Figure 13). On average, the ice speed between 2017 and 2019 increased roughly 50% compared to the preceding two years thus exceeding the speed maxima around the median elevation. The flow acceleration at the terminus is preceded by a terminus retreat along the centerline of $\sim 1.5 \text{ km}$ in summer 2016, concurrent with increased concentration of icebergs in the lake and lake expansion (Figures 14d and 14f). Satellite images reveal that a rift evolved a few kilometers from the terminus (Figure 14f); a large tabular iceberg formed between August 2018 and August 2019 (Figures 14f and 14g) and completely detached in October (Figure 14h) causing further retreat of $\sim 2.2 \text{ km}$ (Figure 13). Since the speedup started before the calving event, we hypothesize that part of the terminus region became buoyant in 2016, that is, well before the large calving event, probably in response to thinning, retreat, and lake expansion which in turn destabilized the terminus area and accelerates ice motion. A similar rapid terminus collapse was observed on nearby Excelsior Glacier in recent years (M. Pelto et al., 2013).

5.5. Comparison With Other Studies

We compare our results to previously published glacier speed data sets that include the Kenai Peninsula's glaciers as part of regional/global-scale ice speed mapping efforts (Figures S8 and S9 in Supporting Information S1).

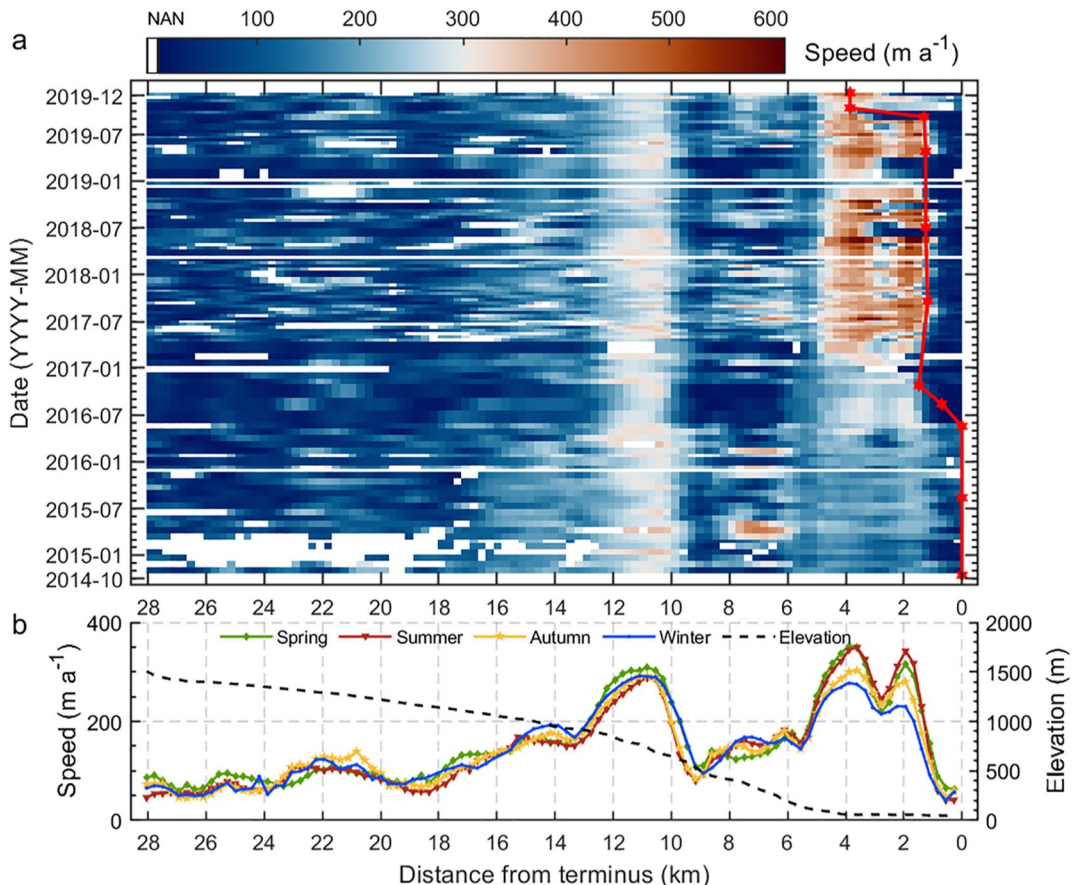


Figure 13. Temporal evolution of the surface speed profile of Ellsworth Glacier. As in Figure 4, the speed variation on the centerline is shown in panel (a), and the averaged seasonal variations are in panel (b). The red line marks the location of the glacier terminus.

Burgess et al. (2013) derived an average mosaicked speed map on a 90×90 m grid over 2007–2010 using offset tracking on Synthetic Aperture Radar Mission ALOS PALSAR (L-Band) image, however, their spatial coverage is only 64%, and results are not directly comparable due to the different time periods. Nevertheless, their spatial variations in surface speed especially over the fastest-flowing tidewater glacier termini compare well with our results. The NASA MEaSUREs ITS_LIVE project (Gardner et al., 2020) provided annual speed data on a 240×240 m grid with almost full spatial coverage using auto-RIFT on Landsat (4, 5, 7, and 8) images (Gardner et al., 2018). Their mean surface ice speed over the entire domain and the 2015–2018 period is 40 m a^{-1} and thus less than our results over the same period (64 m a^{-1}). However, their speed maxima over the fastest-flowing tidewater glaciers (Aialak, Cheneaga) reach almost $1,600 \text{ m a}^{-1}$ which is almost three times faster than our results (Figure S9 in Supporting Information S1). This is consistent with observations on Svalbard by Friedl et al. (2021) who also found higher ITS_LIVE speeds over glacier fronts and shear zones. GoLIVE released speed fields with 300×300 m grid with 16-day resolution at the National Snow and Ice Data Center (Scambos et al., 2016), but their spatial coverage is less than 30% of the Kenai Peninsula glaciers thus hampering comparison to our results.

6. Conclusions

In this study, we applied offset tracking based on 92 pairs of Sentinel-1 data with 12–54 days separation to generate large-scale surface speed fields for the period October 2014 to December 2019 with unprecedented spatial and temporal resolution and coverage for the $3,900 \text{ km}^2$ of glacier ice on the Kenai Peninsula. The data set enabled us to evaluate differences and similarities in seasonal and spatial variations across a larger glacier region, and in particular assess systematically the differences between land-, lake-, and marine-terminating glaciers.

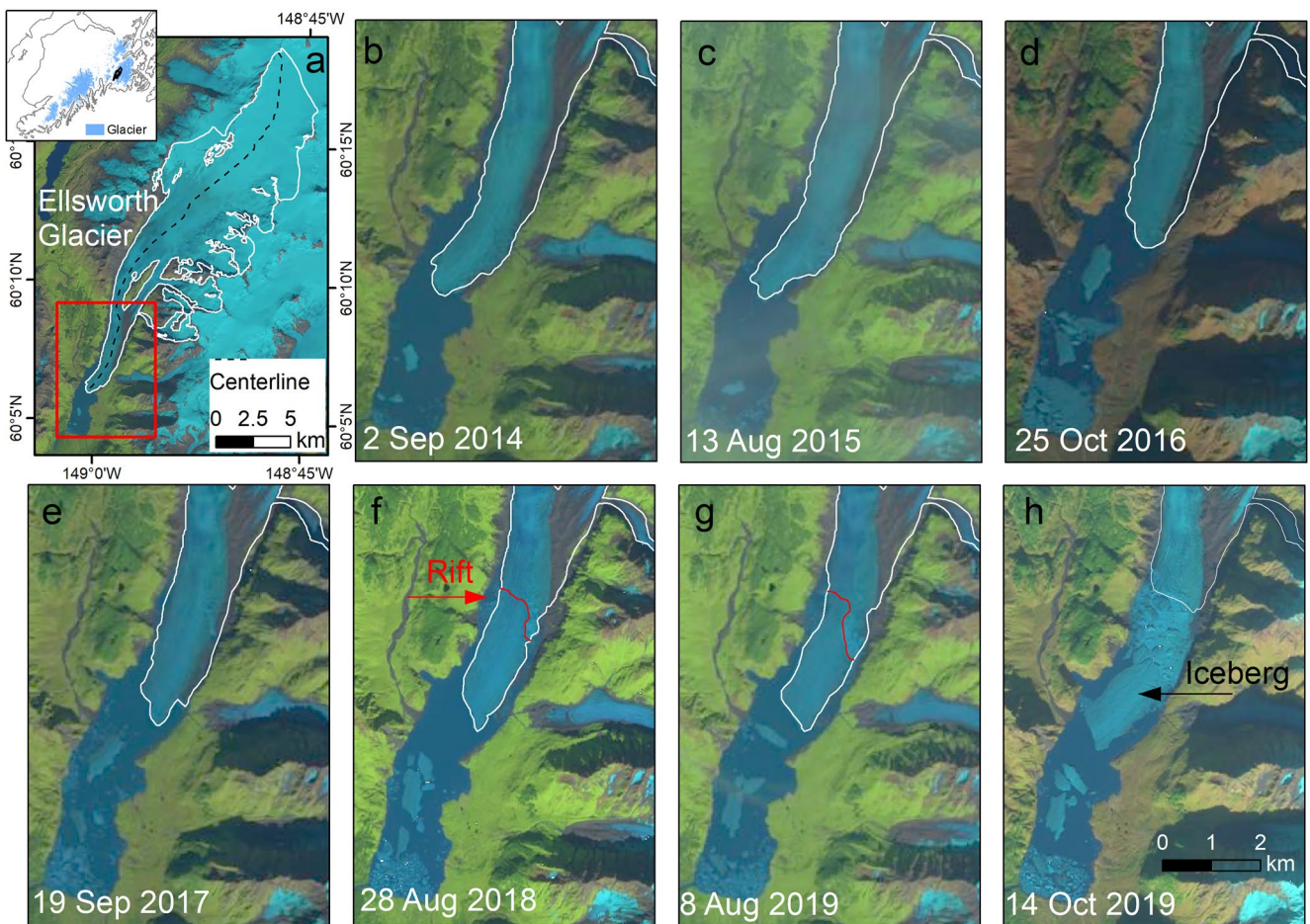


Figure 14. Terminus changes of Ellsworth Glacier 2014–2019. (a) Glacier map, with inset map showing the location of the glacier on the Kenai Peninsula. (b–h) Terminus positions of the area marked by the red rectangle in panel (a). A rift formed between 19 September 2017 (e) and 28 August 2018 (f), while a large iceberg downstream of the rift detached between 8 August 2019 (g) and 14 October 2019 (h). Background images are from Landsat-8 acquired on the dates shown in each map, except panel (h) which is a Sentinel-2 image.

Surface ice speeds averaged over the study period varied between 9 and 600 m a⁻¹ across the Peninsula with an average of roughly 70 m a⁻¹. Generally, most glaciers in this region showed clear seasonal variations including a pronounced spring speedup (with the March-May average more than 50% greater than the annual mean), with a maximum speed in May followed by a minimum in September/October and a second peak in November, while winter speeds are close to the annual mean. We find no trend in interannual mean speed but note that our study period of 5 years may be insufficiently long to detect any longer-term slowdown in response to glacier thinning as observed elsewhere (Dehecq et al., 2019). Short-term variations in speed are remarkably synchronous across the domain suggesting that large-scale climate drivers cause spatially coherent variations in water input. We could not find any correlation between air temperature/precipitation and ice speed. However, detailed distributed mass-balance modeling is needed to provide reliable high-resolution estimates of water input from melt and rain that can be used to study the causes of the spatially coherent speed variations.

We find significant differences in the spatial and temporal speed variations between glaciers of different terminus type. On average, the tidewater glaciers are considerably faster than the lake-terminating glaciers, which in turn are faster than the land-terminating glaciers. The longitudinal speed profiles of the lake-terminating glaciers resemble those of land-terminating glaciers with pronounced maxima around the median glacier elevation while tidewater glaciers have their maxima near the terminus.

Our high-resolution surface speed fields allowed us to detect and evaluate anomalous glacier behavior. We detected a rapid threefold short-term increase in speed of the area below an ice-dammed lake at Bear Glacier in

fall 2019 coincident with an observed GLOF. In contrast our data do not reveal any marked increase in speed in response to an observed GLOF at Bear Glacier in 2018 and at Skilak Glacier in 2016/2018. While physical explanations are possible, this may also highlight the limitations in using Sentinel-1-derived ice speed data to detect GLOFs since short-term speed spikes may go undetected if the image pair separation is too long.

An overall persistent increase in speed of the lower glacier part over the study period is found at both Bear Glacier and Ellsworth Glacier but attributed to different mechanism. At Bear Glacier the speedup followed the breach of the beach barrier between the proglacial lake and the ocean in response to a GLOF in 2018 thus causing inflow of ocean water into the lake. At Ellsworth Glacier rapid glacier retreat and proglacial lake expansion caused the terminus to become buoyant causing a large tabular iceberg to break off and the glacier to speed up.

Overall, our study highlights the potential of high-resolution speed fields to study large-scale glacier behavior and to investigate the connections between speed variations and unusual events such as GLOFs. Our data will also be useful to constrain glacier mass-balance and ice flow models as well as models to invert ice thicknesses.

Data Availability Statement

Sentinel-1 data are freely available at the Alaska Satellite Facility of University of Alaska, Fairbanks (<https://search.asf.alaska.edu/>). The TerraSAR-X data were provided by the German Aerospace Center (DLR) under the project NTI_BIST3395. GAMMA Remote Sensing is a commercial software (<https://www.gamma-rs.ch/>). IFSAR DEM, glacier centerlines, and meteorological data used in this study are listed in the references. Glacier outlines, mean annual/seasonal surface ice speed fields, and speed profiles for 77 glaciers can be accessed at <https://data.mendeley.com/datasets/g3s7m78zk9/draft?a=5086fd51-9c29-476f-aebc-b701c87f7036>. The speed profile code is available at https://github.com/Ruitangtang/Hovemoller_velocity.git. The scientific color map vik is used in this manuscript (Crameri et al., 2020).

Acknowledgments

Support for this work was provided by the Chinese Academy of Sciences (131B62KYSB20180003, QYZDY-SSW-DQC021, and QYZDJ-SSW-DQC039). R. Yang was also funded by the China Scholarship Council. This research was started when R. Yang was a visiting scientist at the University of Alaska Fairbanks. The authors thank Deborah Kurtz from the National Park Service (Kenai Fjords, Alaska, USA) for providing valuable information on Bear Glacier's previous work and Martin Truffer (UAF) for additional input. The authors appreciate all the members in Glacier Group at GI, UAF, and the GeoHyd Group in the Department of Geosciences, UIO, for their kind support and valuable suggestions on this work. The authors declare that they have no conflict of interest. The authors thank the editor Dr. Olga Sergienko, Dr. Bas Altena, Dr. William Armstrong, and two anonymous reviewers for constructive comments which improved the manuscript.

References

- Ahlstrøm, A. P., Andersen, S. B., Andersen, M. L., Machguth, H., Nick, F. M., Joughin, I., et al. (2013). Seasonal velocities of eight major marine-terminating outlet glaciers of the Greenland ice sheet from continuous in situ GPS instruments. *Earth System Science Data*, 5(2), 277–287. <https://doi.org/10.5194/essd-5-277-2013>
- Altena, B., Scambos, T., Fahnestock, M., & Kääb, A. (2019). Extracting recent short-term glacier velocity evolution over southern Alaska and the Yukon from a large collection of Landsat data. *The Cryosphere*, 13(3), 795–814. <https://doi.org/10.5194/tc-13-795-2019>
- Armstrong, W. H., Anderson, R. S., & Fahnestock, M. A. (2017). Spatial patterns of summer speedup on south central Alaska Glaciers. *Geophysical Research Letters*, 44(18), 9379–9388. <https://doi.org/10.1002/2017gl074370>
- Bartholomaus, T. C., Anderson, R. S., & Anderson, S. P. (2008). Response of glacier basal motion to transient water storage. *Nature Geoscience*, 1, 33–37. <https://doi.org/10.1038/ngeo.2007.52>
- Baurley, N. R., Robson, B. A., & Hart, J. K. (2020). Long-term impact of the proglacial lake Jökulsárlón on the flow velocity and stability of Breiðamerkurjökull glacier, Iceland. *Earth Surface Processes and Landforms*, 45(11), 2647–2663. <https://doi.org/10.1002/esp.4920>
- Braithwaite, R. J., & Raper, S. C. B. (2009). Estimating Equilibrium-Line Altitude (ELA) from glacier inventory data. *Annals of Glaciology*, 50(53), 127–132. <https://doi.org/10.3189/172756410790595930>
- Brcic, R., Parizzi, A., Eineder, M., Bamler, R., & Meyer, F. (2011). *Ionospheric effects in SAR interferometry: An analysis and comparison of methods for their estimation*. Paper presented at 2011 IEEE International Geoscience and Remote Sensing Symposium.
- Burgess, E., Forster, R., Larsen, C., & Braun, M. (2012). Surge dynamics on Bering Glacier, Alaska, in 2008–2011. *The Cryosphere*, 6(6), 1251–1262. <https://doi.org/10.5194/tc-6-1251-2012>
- Burgess, E. W., Forster, R. R., & Larsen, C. F. (2013). Flow velocities of Alaskan glaciers. *Nature Communications*, 4(1), 2146. <https://doi.org/10.1038/ncomms3146>
- Casu, F., Manconi, A., Pepe, A., & Lanari, R. (2011). Deformation time-series generation in areas characterized by large displacement dynamics: The SAR amplitude pixel-offset SBAS technique. *IEEE Transactions on Geoscience and Remote Sensing*, 49(7), 2752–2763. <https://doi.org/10.1109/tgrs.2010.2104325>
- Crameri, F., Shephard, G. E., & Heron, P. J. (2020). The misuse of colour in science communication. *Nature Communications*, 11(1), 5444. <https://doi.org/10.1038/s41467-020-19160-7>
- Dall, J., Kusk, A., Nielsen, U. D., & Boncori, J. P. M. (2015). Ice velocity mapping using TOPS SAR data and offset tracking. In *Proceedings of Fringe 2015 Workshop*.
- Davison, B. J., Sole, A. J., Cowton, T. R., Lea, J. M., Slater, D. A., Fahrner, D., & Nienow, P. W. (2020). Subglacial drainage evolution modulates seasonal ice flow variability of three tidewater glaciers in Southwest Greenland. *Journal of Geophysical Research: Earth Surface*, 125(9). <https://doi.org/10.1029/2019jf005492>
- Dehecq, A., Gourmelen, N., Gardner, A. S., Brun, F., Goldberg, D., Nienow, P. W., et al. (2019). Twenty-first century glacier slowdown driven by mass loss in High Mountain Asia. *Nature Geoscience*, 12(1), 22–27. <https://doi.org/10.1038/s41561-018-0271-9>
- Fahnestock, M., Scambos, T., Moon, T., Gardner, A., Haran, T., & Klinger, M. (2016). Rapid large-area mapping of ice flow using Landsat 8. *Remote Sensing of Environment*, 185, 84–94. <https://doi.org/10.1016/j.rse.2015.11.023>
- Farinotti, D., Huss, M., Fürst, J. J., Landmann, J., Machguth, H., Maussion, F., & Pandit, A. (2019). A consensus estimate for the ice thickness distribution of all glaciers on Earth. *Nature Geoscience*, 12(3), 168–173. <https://doi.org/10.1038/s41561-019-0300-3>

- Friedl, P., Seehaus, T., & Braun, M. (2021). Global time series and temporal mosaics of glacier surface velocities derived from Sentinel-1 data. *Earth System Science Data*, 13(10), 4653–4675. <https://doi.org/10.5194/essd-13-4653-2021>
- Fudge, T. J., Harper, J. T., Humphrey, N. F., & Pfeffer, W. T. (2009). Rapid glacier sliding, reverse ice motion and subglacial water pressure during an autumn rainstorm. *Annals of Glaciology*, 50(52), 101–108. <https://doi.org/10.3189/172756409789624247>
- Gardner, A. S., Fahnestock, M. A., & Scambos, T. A. (2020). *ITS_LIVE regional glacier and ice sheet surface velocities*. Data archived at National Snow and Ice Data Center. <https://doi.org/10.5067/6II6VW8LLWJ7>
- Gardner, A. S., Moholdt, G., Scambos, T., Fahnestock, M., Ligtenberg, S., van den Broeke, M., & Nilsson, J. (2018). Increased West Antarctic and unchanged East Antarctic ice discharge over the last 7 years. *The Cryosphere*, 12(2), 521–547. <https://doi.org/10.5194/tc-12-521-2018>
- Giffen, B. A. H., Chien, D. K., & Janet, Y. L. (2007). *Alaska: Glaciers of Kenai Fjords National Park and Katmai National Park and Preserve (Chapter 12)*. Paper presented at 64th Annual Meeting of the Eastern Snow Conference (ESC).
- Gourmelen, N., Kim, S. W., Shepherd, A., Park, J. W., Sundal, A. V., Björnsson, H., & Pálsson, F. (2011). Ice velocity determined using conventional and multiple-aperture InSAR. *Earth and Planetary Science Letters*, 307(1–2), 156–160. <https://doi.org/10.1016/j.epsl.2011.04.026>
- Gray, A. L., Mattar, K. E., & Sofko, G. (2000). Influence of ionospheric electron density fluctuations on satellite radar interferometry. *Geophysical Research Letters*, 27(10), 1451–1454. <https://doi.org/10.1029/2000gl000016>
- Heid, T., & Kääb, A. (2012). Evaluation of existing image matching methods for deriving glacier surface displacements globally from optical satellite imagery. *Remote Sensing of Environment*, 118, 339–355. <https://doi.org/10.1016/j.rse.2011.11.024>
- Howat, I. M., Joughin, I., & Scambos, T. A. (2007). Rapid changes in ice discharge from Greenland outlet glaciers. *Science*, 315(5818), 1559–1561. <https://doi.org/10.1126/science.1138478>
- Iken, A. (1981). The effect of the subglacial water pressure on the sliding velocity of a glacier in an idealized numerical model. *Journal of Glaciology*, 27(97), 407–421. <https://doi.org/10.3189/S0022143000011448>
- Iken, A., & Bindschadler, R. A. (1986). Combined measurements of subglacial water pressure and surface velocity of Findelengletscher, Switzerland: Conclusions about drainage system and sliding mechanism. *Journal of Glaciology*, 32(110), 101–119. <https://doi.org/10.3189/S0022143000006936>
- Iken, A., Röthlisberger, H., Flotron, A., & Haeberli, W. (1983). The uplift of Unteraargletscher at the beginning of the melt season—A consequence of water storage at the bed? *Journal of Glaciology*, 29(101), 28–47. <https://doi.org/10.3189/S002214300005128>
- Jawak, S. D., Kumar, S., Luis, A. J., Pandit, P. H., Wankhede, S. F., & Anirudh, T. S. (2019). Seasonal comparison of velocity of the eastern tributary Glaciers, Amery Ice Shelf, Antarctica, using SAR offset tracking. *ISPRS Annals of Photogrammetry, Remote Sensing and Spatial Information Sciences*, IV-2/W5, 595–600. <https://doi.org/10.5194/isprs-annals-IV-2-W5-595-2019>
- Joughin, I., Abdalati, W., & Fahnestock, M. (2004). Large fluctuations in speed on Greenland's Jakobshavn Isbrae glacier. *Nature*, 432(7017), 608–610. <https://doi.org/10.1038/nature03130>
- Joughin, I., Howat, I., Alley, R. B., Ekstrom, G., Fahnestock, M., Moon, T., et al. (2008). Ice-front variation and tidewater behavior on Helheim and Kangerdlugssuaq Glaciers, Greenland. *Journal of Geophysical Research*, 113(F1), F01004. <https://doi.org/10.1029/2007JF000837>
- Joughin, I., Smith, B. E., & Abdalati, W. (2010). Glaciological advances made with Interferometric Synthetic Aperture Radar. *Journal of Glaciology*, 56(200), 1026–1042. <https://doi.org/10.3189/002214311796406158>
- Joughin, I., Smith, B. E., & Howat, I. (2018). Greenland Ice Mapping Project: Ice flow velocity variation at sub-monthly to decadal timescales. *The Cryosphere*, 12(7), 2211–2227. <https://doi.org/10.5194/tc-12-2211-2018>
- Kääb, A. (2005). Combination of SRTM3 and repeat ASTER data for deriving alpine glacier flow velocities in the Bhutan Himalaya. *Remote Sensing of Environment*, 94(4), 463–474. <https://doi.org/10.1016/j.rse.2004.11.003>
- Kamb, B. (1987). Glacier surge mechanism based on linked cavity configuration of the basal water conduit system. *Journal of Geophysical Research*, 92(B9), 9083–9100. <https://doi.org/10.1029/JB092iB09p09083>
- Kumar, V., Venkataraman, G., Högda, K. A., & Larsen, Y. (2013). Estimation and validation of glacier surface motion in the northwestern Himalayas using high-resolution SAR intensity tracking. *International Journal of Remote Sensing*, 34(15), 5518–5529. <https://doi.org/10.1080/01431161.2013.792965>
- Kumar, V., Venkataramana, G., & Högda, K. A. (2011). Glacier surface velocity estimation using SAR interferometry technique applying ascending and descending passes in Himalayas. *International Journal of Applied Earth Observation and Geoinformation*, 13(4), 545–551. <https://doi.org/10.1016/j.jag.2011.02.004>
- Kurtz, D., & Wolken, G. (2019). Risk and recreation in a glacial environment: Understanding glacial lake outburst floods at Bear Glacier in Kenai fjords national Park. *Alaska Park Science*, 18(1), 38–43.
- Lanik, A., Hults, C. P., & Kurtz, D. (2018). *Kenai Fjords National Park: Geologic resources inventory report* (Natural Resource Report NPS/NRSS/GRD/NRR–2018/1851). National Park Service.
- Le Bris, R., Paul, F., Frey, H., & Bolch, T. (2011). A new satellite-derived glacier inventory for Western Alaska. *Annals of Glaciology*, 52(59), 135–143. <https://doi.org/10.3189/172756411799096303>
- Lemos, A., Shepherd, A., McMillan, M., Hogg, A. E., Hatton, E., & Joughin, I. (2018). Ice velocity of Jakobshavn Isbrae, Petermann Glacier, Nioghalvfjerdsfjorden, and Zachariae Isström, 2015–2017, from Sentinel 1-a/b SAR imagery. *The Cryosphere*, 12(6), 2087–2097. <https://doi.org/10.5194/tc-12-2087-2018>
- Luckman, A., Quincey, D., & Bevan, S. (2007). The potential of satellite radar interferometry and feature tracking for monitoring flow rates of Himalayan glaciers. *Remote Sensing of Environment*, 111(2–3), 172–181. <https://doi.org/10.1016/j.rse.2007.05.019>
- Magnússon, E., Rott, H., Björnsson, H., & Pálsson, F. (2007). The impact of jökulhlaups on basal sliding observed by SAR interferometry on Vatnajökull, Iceland. *Journal of Glaciology*, 53(181), 232–240. <https://doi.org/10.3189/172756507782202810>
- Mair, D., Nienow, P., Willis, I., & Sharp, M. (2001). Spatial patterns of glacier motion during a high-velocity event: Haut Glacier d'Arolla, Switzerland. *Journal of Glaciology*, 47(156), 9–20. <https://doi.org/10.3189/172756501781832412>
- McNabb, R. W., Hock, R., & Huss, M. (2015). Variations in Alaska tidewater glacier frontal ablation, 1985–2013. *Journal of Geophysical Research*, 120(1), 120–136. <https://doi.org/10.1002/2014JF003276>
- McNabb, R. W., Hock, R., O'Neal, S., Rasmussen, L., Ahn, Y., Braun, M., et al. (2012). Using surface velocities to calculate ice thickness and bed topography: A case study at Columbia Glacier, Alaska, USA. *Journal of Glaciology*, 58(212), 1151–1164. <https://doi.org/10.3189/2012JG11J249>
- Meier, M. F., & Post, A. (1987). Fast tidewater glaciers. *Journal of Geophysical Research*, 92(B9), 9051–9058. <https://doi.org/10.1029/jb092ib09p09051>
- Melkonian, A. K., Willis, M. J., & Pritchard, M. E. (2014). Satellite-derived volume loss rates and glacier speeds for the Juneau Icefield, Alaska. *Journal of Glaciology*, 60(222), 743–760. <https://doi.org/10.3189/2014JG13J181>
- Michel, R., & Rignot, E. (1999). Flow of Glaciar Moreno, Argentina, from repeat-pass Shuttle Imaging radar images: Comparison of the phase correlation method with radar interferometry. *Journal of Glaciology*, 45(149), 93–100. <https://doi.org/10.3189/s0022143000003075>

- Millan, R., Mouginot, J., Rabatel, A., Jeong, S., Cusicanqui, D., Derkacheva, A., & Chekki, M. (2019). Mapping surface flow velocity of glaciers at regional scale using a multiple sensors approach. *Remote Sensing*, 11(21), 2498. <https://doi.org/10.3390/rs11212498>
- Millan, R., Mouginot, J., Rabatel, A., & Morlighem, M. (2022). Ice velocity and thickness of the world's glaciers. *Nature Geoscience*, 15(2), 124–129. <https://doi.org/10.1038/s41561-021-00885-z>
- Moon, T., Joughin, I., & Smith, B. (2015). Seasonal to multiyear variability of glacier surface velocity, terminus position, and sea ice/ice mélange in northwest Greenland. *Journal of Geophysical Research: Earth Surface*, 120(5), 818–833. <https://doi.org/10.1002/2015jf003494>
- Moon, T., Joughin, I., Smith, B., Van Den Broeke, M. R., Van De Berg, W. J., Noël, B., & Usher, M. (2014). Distinct patterns of seasonal Greenland glacier velocity. *Geophysical Research Letters*, 41(20), 7209–7216. <https://doi.org/10.1002/2014gl061836>
- Mouginot, J., & Rignot, E. (2015). Ice motion of the Patagonian Icefields of south America: 1984–2014. *Geophysical Research Letters*, 42(5), 1441–1449. <https://doi.org/10.1002/2014gl062661>
- Mouginot, J., Rignot, E., Scheuchl, B., & Millan, R. (2017). Comprehensive annual ice sheet velocity mapping using Landsat-8, Sentinel-1, and RADARSAT-2 data. *Remote Sensing*, 9(4), 364. <https://doi.org/10.3390/rs9040364>
- Muto, M., & Furuya, M. (2013). Surface velocities and ice-front positions of eight major glaciers in the Southern Patagonian Ice Field, South America, from 2002 to 2011. *Remote Sensing of Environment*, 139, 50–59. <https://doi.org/10.1016/j.rse.2013.07.034>
- Nagler, T., Rott, H., Hetzenecker, M., Wuite, J., & Potin, P. (2015). The Sentinel-1 mission: New opportunities for ice sheet observations. *Remote Sensing*, 7(7), 9371–9389. <https://doi.org/10.3390/rs70709371>
- Neelmeijer, J., Motagh, M., & Wetzel, H.-U. (2014). Estimating spatial and temporal variability in surface kinematics of the Inylchek Glacier, central Asia, using TerraSAR-X data. *Remote Sensing*, 6(10), 9239–9259. <https://doi.org/10.3390/rs6109239>
- O'Neal, S., Echelmeyer, K. A., & Motyka, R. J. (2001). Short-term flow dynamics of a retreating tidewater glacier: LeConte Glacier, Alaska, U.S.A. *Journal of Glaciology*, 47(159), 567–578. <https://doi.org/10.3189/172756501781831855>
- O'Neal, S., Pfeffer, W. T., Krimmel, R., & Meier, M. (2005). Evolving force balance at Columbia Glacier, Alaska, during its rapid retreat. *Journal of Geophysical Research*, 110(F3), F03012. <https://doi.org/10.1029/2005JF000292>
- Osmanoglu, B., Braun, M., Hock, R., & Navarro, F. (2013). Surface velocity and ice discharge of the ice cap on King George Island, Antarctica. *Annals of Glaciology*, 54(63), 111–119. <https://doi.org/10.3189/2013aog63a517>
- Osmanoglu, B., Navarro, F. J., Hock, R., Braun, M., & Corcuera, M. I. (2014). Surface velocity and mass balance of Livingston Island ice cap, Antarctica. *The Cryosphere*, 8(5), 1807–1823. <https://doi.org/10.5194/tc-8-1807-2014>
- Paul, F., Bolch, T., Briggs, K., Kaab, A., McMillan, M., McNabb, R., et al. (2017). Error sources and guidelines for quality assessment of glacier area, elevation change, and velocity products derived from satellite data in the Glaciers_cci project. *Remote Sensing of Environment*, 203, 256–275. <https://doi.org/10.1016/j.rse.2017.08.038>
- Paul, F., Bolch, T., Kaab, A., Nagler, T., Nuth, C., Scharrer, K., et al. (2015). The glaciers climate change initiative: Methods for creating glacier area, elevation change and velocity products. *Remote Sensing of Environment*, 162, 408–426. <https://doi.org/10.1016/j.rse.2013.07.043>
- Pelto, M., Capps, D., Clague, J. J., & Pelto, B. (2013). Rising ELA and expanding proglacial lakes indicate impending rapid retreat of Brady Glacier, Alaska. *Hydrological Processes*, 27(21), 3075–3082. <https://doi.org/10.1002/hyp.9913>
- Pelto, M. S., Miller, M. M., Adema, G. W., Beedle, M. J., McGee, S. R., Sprenke, K. F., & Lang, M. (2008). The equilibrium flow and mass balance of the Taku Glacier, Alaska 1950–2006. *The Cryosphere*, 2, 147–157. <https://doi.org/10.5194/tc-2-147-2008>
- Pritchard, H. D., & Vaughan, D. G. (2007). Widespread acceleration of tidewater glaciers on the Antarctic Peninsula. *Journal of Geophysical Research*, 112(F3), F03S29. <https://doi.org/10.1029/2006JF000597>
- Purdie, H. L., Brook, M. S., & Fuller, I. C. (2008). Seasonal variation in ablation and surface velocity on a temperate maritime glacier: Fox Glacier, New Zealand. *Arctic Antarctic and Alpine Research*, 40(1), 140–147. [https://doi.org/10.1657/1523-0430\(06-032\)purdie2.0.Co;2](https://doi.org/10.1657/1523-0430(06-032)purdie2.0.Co;2)
- Rankl, M., Kienholz, C., & Braun, M. (2014). Glacier changes in the Karakoram region mapped by multimission satellite imagery. *The Cryosphere*, 8(3), 977–989. <https://doi.org/10.5194/tc-8-977-2014>
- RGI Consortium. (2017). *Randolph Glacier Inventory – A dataset of global glacier outlines: Version 6.0: Technical report, global land ice measurements from Space*. Digital Media. <https://doi.org/10.7265/N5-RGI-60>
- Rignot, E., Forster, R., & Isacks, B. (1996). Interferometric radar observations of Glaciar San Rafael, Chile. *Journal of Glaciology*, 42(141), 279–291. <https://doi.org/10.3189/S002214300004147>
- Rignot, E., & Mouginot, J. (2012). Ice flow in Greenland for the International Polar Year 2008–2009. *Geophysical Research Letters*, 39(11). <https://doi.org/10.1029/2012gl051634>
- Rohner, C., Small, D., Beutel, J., Henke, D., Lüthi, M. P., & Vieli, A. (2019). Multisensor validation of tidewater glacier flow fields derived from synthetic aperture radar (SAR) intensity tracking. *The Cryosphere*, 13(11), 2953–2975. <https://doi.org/10.5194/tc-13-2953-2019>
- Rosenau, R., Scheinert, M., & Dietrich, R. (2015). A processing system to monitor Greenland outlet glacier velocity variations at decadal and seasonal time scales utilizing the Landsat imagery. *Remote Sensing of Environment*, 169, 1–19. <https://doi.org/10.1016/j.rse.2015.07.012>
- Röhlisberger, H. (1972). Water pressure in intra- and subglacial channels. *Journal of Glaciology*, 11(62), 177–203. <https://doi.org/10.3189/S0022143000022188>
- Rousseeuw, P. J., & Croux, C. (1993). Alternatives to the median absolute deviation. *Journal of the American Statistical Association*, 88(424), 1273–1283. <https://doi.org/10.1080/01621459.1993.10476408>
- Sakakibara, D., & Sugiyama, S. (2018). Ice front and flow speed variations of marine-terminating outlet glaciers along the coast of Prudhoe Land, northwestern Greenland. *Journal of Glaciology*, 64(244), 300–310. <https://doi.org/10.1017/jog.2018.20>
- Sakakibara, D., Sugiyama, S., Sawagaki, T., Marinsek, S., & Skvarca, P. (2013). Rapid retreat, acceleration and thinning of Glaciar Upsala, Southern Patagonia Icefield, initiated in 2008. *Annals of Glaciology*, 54(63), 131–138. <https://doi.org/10.3189/2013AoG63A236>
- Sánchez-Gámez, P., & Navarro, F. (2017). Glacier surface velocity retrieval using D-InSAR and offset tracking techniques applied to ascending and descending passes of Sentinel-1 data for southern Ellesmere ice caps, Canadian Arctic. *Remote Sensing*, 9(5), 442. <https://doi.org/10.3390/rs9050442>
- Sansosti, E., Berardino, P., Manunta, M., Serafino, F., & Fornaro, G. (2006). Geometrical SAR image registration. *IEEE Transactions on Geoscience and Remote Sensing*, 44(10), 2861–2870. <https://doi.org/10.1109/tgrs.2006.875787>
- Satyabala, S. P. (2016). Spatiotemporal variations in surface velocity of the Gangotri glacier, Garhwal Himalaya, India: Study using synthetic aperture radar data. *Remote Sensing of Environment*, 181, 151–161. <https://doi.org/10.1016/j.rse.2016.03.042>
- Scambos, T., Fahnestock, M., Moon, T., Gardner, A., & Klingler, M. (2016). *Global Land Ice Velocity Extraction from Landsat 8 (GoLIVE)*, version 1. NSIDC: National Snow and Ice Data Center. <https://doi.org/10.7265/N5ZP442B>
- Schellenberger, T., Dunse, T., Kääb, A., Kohler, J., & Reijmer, C. H. (2015). Surface speed and frontal ablation of Kronebreen and Kongsbreen, NW Svalbard, from SAR offset tracking. *The Cryosphere*, 9(6), 2339–2355. <https://doi.org/10.5194/tc-9-2339-2015>

- Seehaus, T., Marinsek, S., Helm, V., Skvarca, P., & Braun, M. (2015). Changes in ice dynamics, elevation and mass discharge of Dinsmoor–Bombardier–Edgeworth glacier system, Antarctic Peninsula. *Earth and Planetary Science Letters*, 427, 125–135. <https://doi.org/10.1016/j.epsl.2015.06.047>
- Strozzi, T., Luckman, A., Murray, T., Wegmüller, U., & Werner, C. L. (2002). Glacier motion estimation using SAR offset-tracking procedures. *IEEE Transactions on Geoscience and Remote Sensing*, 40(11), 2384–2391. <https://doi.org/10.1109/tgrs.2002.805079>
- Strozzi, T., Paul, F., Wiesmann, A., Schellenberger, T., & Kääb, A. (2017). Circum-Arctic Changes in the Flow of Glaciers and Ice Caps from Satellite SAR Data between the 1990s and 2017. *Remote Sensing*, 9, 947. <https://doi.org/10.3390/rs9090947>
- Trabant, D. C., Krimmel, R. M., Echelmeyer, K. A., Zirnfeld, S. L., & Elsberg, D. H. (2003). The slow advance of a calving glacier: Hubbard Glacier, Alaska, U.S.A. *Annals of Glaciology*, 36, 45–50. <https://doi.org/10.3189/172756403781816400>
- Truffer, M., & Motyka, R. J. (2016). Where glaciers meet water: Subaqueous melt and its relevance to glaciers in various settings. *Reviews of Geophysics*, 54(1), 220–239. <https://doi.org/10.1002/2015rg000494>
- Trüssel, B. L., Motyka, R. J., Truffer, M., & Larsen, C. F. (2013). Rapid thinning of lake-calving Yakutat Glacier and the collapse of the Yakutat Icefield, southeast Alaska, USA. *Journal of Glaciology*, 59(213), 149–161. <https://doi.org/10.3189/2013j0g12j081>
- Tsutaki, S., Fujita, K., Nuimura, T., Sakai, A., Sugiyama, S., Komori, J., & Tshering, P. (2019). Contrasting thinning patterns between lake- and land-terminating glaciers in the Bhutanese Himalaya. *The Cryosphere*, 13(10), 2733–2750. <https://doi.org/10.5194/tc-13-2733-2019>
- Vallot, D., Pettersson, R., Luckman, A., Benn, D. I., Zwinger, T., Van Pelt, W. J. J., et al. (2017). Basal dynamics of Kronebreen, a fast-flowing tidewater glacier in Svalbard: Non-local spatio-temporal response to water input. *Journal of Glaciology*, 63(242), 1012–1024. <https://doi.org/10.1017/jog.2017.69>
- Van den Broeke, M., Bamber, J., Ettema, J., Rignot, E., Schrama, E., van de Berg, W. J., et al. (2009). Partitioning recent Greenland mass loss. *Science*, 326(5955), 984–986. <https://doi.org/10.1126/science.1178176>
- Van Wychen, W., Burgess, D., Kochtitzky, W., Nikolic, N., Copland, L., & Gray, L. (2020). RADARSAT-2 derived glacier velocities and dynamic discharge estimates for the Canadian High Arctic: 2015–2020. *Canadian Journal of Remote Sensing*, 46(6), 695–714. <https://doi.org/10.1080/07038992.2020.1859359>
- Van Wychen, W., Burgess, D. O., Gray, L., Copland, L., Sharp, M., Dowdeswell, J. A., & Benham, T. J. (2014). Glacier velocities and dynamic ice discharge from the Queen Elizabeth Islands, Nunavut, Canada. *Geophysical Research Letters*, 41(2), 484–490. <https://doi.org/10.1002/2013gl058558>
- Vieli, A., Jania, J., Blatter, H., & Funk, M. (2004). Short-term velocity variations on Hansbreen, a tidewater glacier in Spitsbergen. *Journal of Glaciology*, 50(170), 389–398. <https://doi.org/10.3189/172756504781829963>
- Vijay, S., & Braun, M. (2017). Seasonal and interannual variability of Columbia Glacier, Alaska (2011–2016): Ice velocity, mass flux, surface elevation and front position. *Remote Sensing*, 9(6), 635. <https://doi.org/10.3390/rs9060635>
- Vijay, S., Khan, S. A., Kusk, A., Solgaard, A. M., Moon, T., & Bjørk, A. A. (2019). Resolving seasonal ice velocity of 45 Greenlandic glaciers with very high temporal details. *GRL*, 46(3), 1485–1495. <https://doi.org/10.1029/2018GL081503>
- Walder, J. S. (1986). Hydraulics of subglacial cavities. *Journal of Glaciology*, 32(112), 439–445. <https://doi.org/10.3189/S0022143000012156>
- Wegmüller, U., Werner, C., Strozzi, T., & Wiesmann, A. (2006). Ionospheric electron concentration effects on SAR and INSAR. Paper presented at 2006 IEEE International Symposium on Geoscience and Remote Sensing.
- Wegmüller, U., Werner, C., Strozzi, T., Wiesmann, A., Frey, O., & Santoro, M. (2016). Sentinel-1 support in the GAMMA software. *Procedia Computer Science*, 100, 1305–1312. <https://doi.org/10.1016/j.procs.2016.09.246>
- Wilcox, A. C., Wade, A. A., & Evans, E. G. (2014). Drainage events from a glacier-dammed lake, Bear Glacier, Alaska: Remote sensing and field observations. *Geomorphology*, 220, 41–49. <https://doi.org/10.1016/j.geomorph.2014.05.025>
- Wiles, G. C., & Calkin, P. E. (1992). Reconstruction of a debris-slide-initiated flood in the southern Kenai Mountains, Alaska. *Geomorphology*, 5(6), 535–546. [https://doi.org/10.1016/0169-555X\(92\)90024-I](https://doi.org/10.1016/0169-555X(92)90024-I)
- Willis, I. C. (1995). Intra-annual variations in glacier motion: A review. *Progress in Physical Geography: Earth and Environment*, 19(1), 61–106. <https://doi.org/10.1177/030913339501900104>
- Wu, K., Liu, S., Xu, J., Zhu, Y., Liu, Q., Jiang, Z., & Wei, J. (2020). Spatiotemporal variability of surface velocities of monsoon temperate glaciers in the Kangri Karpo Mountains, southeastern Tibetan Plateau. *Journal of Glaciology*, 67(261), 1–6. <https://doi.org/10.1017/jog.2020.98>
- Yang, R., Hock, R., Kang, S., Shangguan, D., & Guo, W. (2020). Glacier mass and area changes on the Kenai Peninsula, Alaska, 1986–2016. *Journal of Glaciology*, 66(258), 1–15. <https://doi.org/10.1017/jog.2020.32>
- Yasuda, T., & Furuya, M. (2013). Short-term glacier velocity changes at West Kunlun Shan, Northwest Tibet, detected by Synthetic Aperture Radar data. *Remote Sensing of Environment*, 128, 87–106. <https://doi.org/10.1016/j.rse.2012.09.021>
- Zhou, C., Zhou, Y., Deng, F., Ai, S., Wang, Z., & Dongchen, D. E. (2017). Seasonal and interannual ice velocity changes of Polar Record Glacier, East Antarctica. *Annals of Glaciology*, 55(66), 45–51. <https://doi.org/10.3189/2014AoG66A185>